Cell Reports

Article

Directed differentiation of human iPSCs into mesenchymal lineages by optogenetic control of TGF-β signaling

Graphical abstract

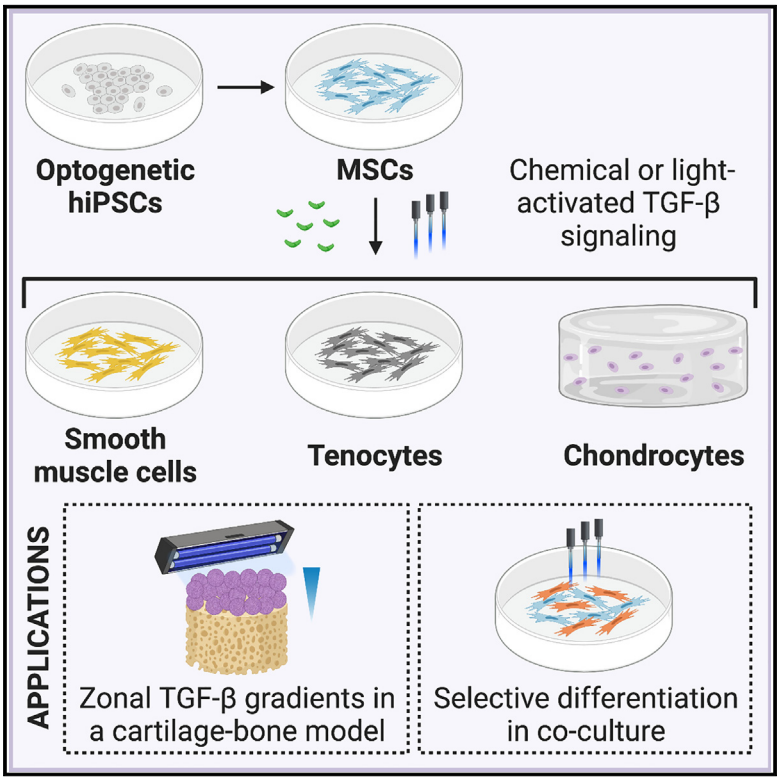

Highlights

- Optogenetic TGF-β signaling in hiPSCs is facilitated by light-activated receptors
- Optogenetic TGF-β signaling directs multilineage mesenchymal differentiations
- Light-patterned TGF-β gradients support organized tissue development
- Selective TGF-β signaling activation enables co-cultures of stem cells and progeny

Authors

Josephine Y. Wu, Keith Yeager, Daniel Naveed Tavakol, ..., Rajesh Kumar Soni, Clark T. Hung, Gordana Vunjak-Novakovic

Correspondence

gv2131@columbia.edu

In brief

Transforming growth factor (TGF)-β signaling modulates key stem cell functions in tissue development and homeostasis. Wu et al. established a human iPSC-based platform for light-activated TGF-β signaling. Leveraging the spatiotemporal precision of light, they applied this tool to support organized tissue development and co-cultures of stem cells and differentiated progeny.

Wu et al., 2023, Cell Reports *42*, 112509
May 30, 2023
https://doi.org/10.1016/j.celrep.2023.112509

CellPress

Cell Reports

CellPress
OPEN ACCESS

Article

Directed differentiation of human iPSCs into mesenchymal lineages by optogenetic control of TGF-β signaling

Josephine Y. Wu,[1] Keith Yeager,[1] Daniel Naveed Tavakol,[1] Margaretha Morsink,[1] Bryan Wang,[2] Rajesh Kumar Soni,[3] Clark T. Hung,[1] and Gordana Vunjak-Novakovic[1,2,4,*]

[1]Department of Biomedical Engineering, Columbia University, New York, NY 10032, USA
[2]Department of Medicine, Columbia University, New York, NY 10032, USA
[3]Proteomics and Macromolecular Crystallography Shared Resource, Herbert Irving Comprehensive Cancer Center, Columbia University, New York, NY 10032, USA
[4]Lead contact
*Correspondence: gv2131@columbia.edu
https://doi.org/10.1016/j.celrep.2023.112509

SUMMARY

In tissue development and homeostasis, transforming growth factor (TGF)-β signaling is finely coordinated by latent forms and matrix sequestration. Optogenetics can offer precise and dynamic control of cell signaling. We report the development of an optogenetic human induced pluripotent stem cell system for TGF-β signaling and demonstrate its utility in directing differentiation into the smooth muscle, tenogenic, and chondrogenic lineages. Light-activated TGF-β signaling resulted in expression of differentiation markers at levels close to those in soluble factor-treated cultures, with minimal phototoxicity. In a cartilage-bone model, light-patterned TGF-β gradients allowed the establishment of hyaline-like layer of cartilage tissue at the articular surface while attenuating with depth to enable hypertrophic induction at the osteochondral interface. By selectively activating TGF-β signaling in co-cultures of light-responsive and non-responsive cells, undifferentiated and differentiated cells were simultaneously maintained in a single culture with shared medium. This platform can enable patient-specific and spatiotemporally precise studies of cellular decision making.

INTRODUCTION

Transforming growth factor (TGF)-β signaling is critical to healthy development and homeostasis, while aberrant signaling has been implicated in pathological conditions such as Marfan syndrome, the related Loeys-Dietz syndrome, various cancers, and fibrosis.[1] TGF-β is known to direct nearly every aspect of mesenchymal stromal/stem cell (MSC) function, including proliferation, immunomodulation, and multilineage differentiation.[2] The regulation of TGF-β signaling is important for a number of organ systems, and as a result, the TGF-β family has been investigated for therapeutic targeting in stem cells and regenerative medicine.

In cell-based cartilage tissue engineering, TGF-β is one of the most widely used mediators to drive chondrogenesis and promote tissue growth.[3] Spatiotemporal gradients of TGF-β signaling are critical to the development of stratified native-like cartilage. Cartilage tissue constructs formed from human bone marrow-derived MSCs under spatiotemporal regulation of TGF-β signaling mimicking native gradients demonstrated improved *in vivo* stability compared with their isotropic control counterparts, resisting endochondral ossification and retaining physiologic stratified organization.[4] In juvenile bovine chondrocytes, brief, rather than sustained, exposure to TGF-β at concentrations lower than the typically applied supraphysiological dose of 10 ng/mL was sufficient for robust cartilage tissue formation.[3,5,6] Other studies that used integrated experimental and computational approaches have shown that TGF-β stimulation can induce short-term graded responses (*Smad7* gene expression) that evolved into long-term switch-like responses (growth inhibition).[7]

Despite abundant studies of the effects of TGF-β signaling in MSCs and their progeny, most stem cell differentiation protocols continue to use a standardized regimen of 10 ng/mL soluble TGF-β with media changes every 3–4 days throughout the culture duration.[4,8,9] Translational potential remains limited, in large part due to variability of both soluble regulatory factors (batch variability, culture stability, spatiotemporal imprecision) and cell sources (non-autologous, with a range of donor ages, tissue origins, and disease states).

In physiological studies *in vivo*, TGF-β signaling is elegantly coordinated by latent forms and matrix sequestration,[5] while the maintenance of gradients of factors *in vitro* is inherently imprecise. This has been well documented for recombinant basic fibroblast growth factor (bFGF, or FGF2), a regulatory protein that maintains the self-renewal and undifferentiated state of human pluripotent stem cells. Standard stem cell maintenance methods require daily replacements of culture medium to

replenish the growth factors. However, FGF2 concentration decreases to 40% of supplemented levels after only 4 h and to 10% after 24 h.[10] Based on these findings, other investigators developed thermostable chimeric variants that enable every-other-day medium changes with sustained, rather than highly fluctuating, FGF concentration profiles.[11,12]

Additional efforts were directed toward developing precise tools for manipulating TGF-β signaling, such as chimeric receptors,[13] synthetic ligand-presenting surfaces,[14] infrared light-released ligands in carbon nanotubes,[15] inhibitors of receptor kinase activity,[16] or ligand-binding inhibitors.[17] Unfortunately, chemical tools cannot exert the levels of spatiotemporal resolution necessary to mimic physiologic TGF-β signaling. In particular, maintenance of a chemically based gradient becomes challenging and cumbersome in complex settings, such as diffusion-limited tissue constructs or organs-on-chip systems with perfusion.

Optogenetics provides a means for inducing cell physiology by light stimulation, offering unprecedented precision and dynamic control of cell signaling in space and time.[18] The photoactivatable proteins driving light responsiveness show rapid reversibility, and spatial patterning by photomasks in optogenetic cell monolayers with resolution on the scale of 100 μm has been demonstrated.[19] To date, optogenetics has been used to interrogate major pathways such as FGF or Wnt/β-catenin, largely in immortalized cell lines and only more recently in pluripotent stem cells.[20–22] Human induced pluripotent stem cells (hiPSCs) can be derived in a minimally invasive and patient-specific manner and are enabling personalized studies of injury, disease, and therapy.

In this study, we aimed to develop hiPSC-derived MSCs capable of optogenetic TGF-β signaling (optohiMSCs), validate the mesenchymal phenotype of the resulting optohiMSCs, and show that light can be used in lieu of soluble growth factor to drive TGF-β-mediated multilineage mesenchymal differentiation, including chondrogenic differentiation in 3D culture. We anticipate that the optogenetically edited cells can serve as a versatile tool for studying and exploiting TGF-β signaling in MSCs.

RESULTS

Study design

Our objective was to establish an hiPSC-based system that would allow the use of light to control TGF-β signaling. We hypothesized that we can stably introduce optogenetic TGF-β receptors into hiPSCs without functional detriment and that light can be used to recapitulate the role of soluble TGF-β in mesenchymal differentiations into smooth muscle, tenogenic, and chondrogenic lineages.

We started by generating clonal hiPSC populations with optogenetic receptors that could activate TGF-β signaling in response to blue light. Canonical TGF-β signaling is initiated at the cell surface when TGF-β binds the transmembrane TGF-β type I and type II receptors (TGFBR1 and TGFBR2, respectively) (Figure 1A). The resulting cascade of phosphorylation events leads to the nuclear localization of a Smad complex that regulates gene expression.[23] In the light-inducible system previously developed,[24] signaling was mediated by the blue light activation of *Arabidopsis thaliana* protein interactions between the truncated N-terminal end of cryptochrome-interacting basic-helix-loop-helix 1 (CIBN) and cryptochrome 2 (CRY2), with each protein being coupled to a receptor. The optogenetic TGFBR1 (optoTGFBR1) was comprised of a myristoylation signal peptide (Myr) tether to the plasma membrane, the intracellular region of native TGFBR1, and CIBN. The optoTGFBR2 was comprised of the intracellular region of native TGFBR2, CRY2, and a tdTomato fluorescent tag (Figure 1B).

The subsequent generation of optohiMSCs—validated for mesenchymal potential using the standard criteria of adherence to uncoated tissue culture plastic with elongated morphology, expression of appropriate cell surface markers, and tri-differentiation into adipogenic, osteogenic, and chondrogenic lineages[25]—served two main purposes. First, it provided functional validation that the introduction of the optogenetic system into hiPSCs did not affect their ability to differentiate into other cell types. Second, the optohiMSCs were the starting point for downstream differentiations into smooth muscle, tenogenic, and chondrogenic lineages. TGF-β is known to be a potent regulator in differentiations of MSCs, and the transcription factors through which it acts have been identified.[2]

MSC differentiations span a range of complexity: where the derivation of smooth muscle cells largely depends on TGF-β and stiff substrate,[8] tenocytes require stepwise supplementation with additional growth factors beyond TGF-β,[9] and chondrocytes need to be cultured in 3D settings.[26] For each differentiation, we compared groups that received no soluble TGF-β or optogenetic stimulation (−T) with those receiving soluble TGF-β3 alone (+T) or optogenetic stimulation alone at two intensities of light (+L3 or +L6), keeping all other culture conditions the same. The effects of TGF-β signaling on these MSC differentiations, assessed by qRT-PCR, immunostaining, and global quantitative proteomics, were used to demonstrate that light-activated TGF-β signaling can drive biologically meaningful responses beyond the previously shown upstream characterization of optogenetic receptor behavior.[24]

Generation of hiPSC lines allowing optogenetic control of TGF-β signaling

Prior reports had developed optogenetic TGF-β receptors and characterized light-activated signaling in the immortalized and highly durable HeLa cell line.[24] Here, we established the optogenetic system for use in hiPSCs via lentiviral transduction, suitable for both dividing and non-dividing cells without causing tumorigenic effects. To this end, we developed a single construct containing the two optoTGFBRs with the human elongation factor (EF)-1α promoter in order to achieve the constitutive and long-term expression (Figures 1C and S1).[27] The resulting hiPSC lines were stable and had capability for light activation of TGF-β signaling (optohiPSCs). In clonally expanded populations, optohiPSCs robustly expressed the tdTomato-tagged optogenetic system, maintained their pluripotency, and featured a normal karyotype (Figures 1D, 1E, and S2).

MSCs derived from optohiPSCs maintain phenotype and light responsiveness

Following mesenchymal differentiation, the optohiMSCs adhered to uncoated standard tissue culture plastic with elongated morphology while maintaining high expression of optogenetic

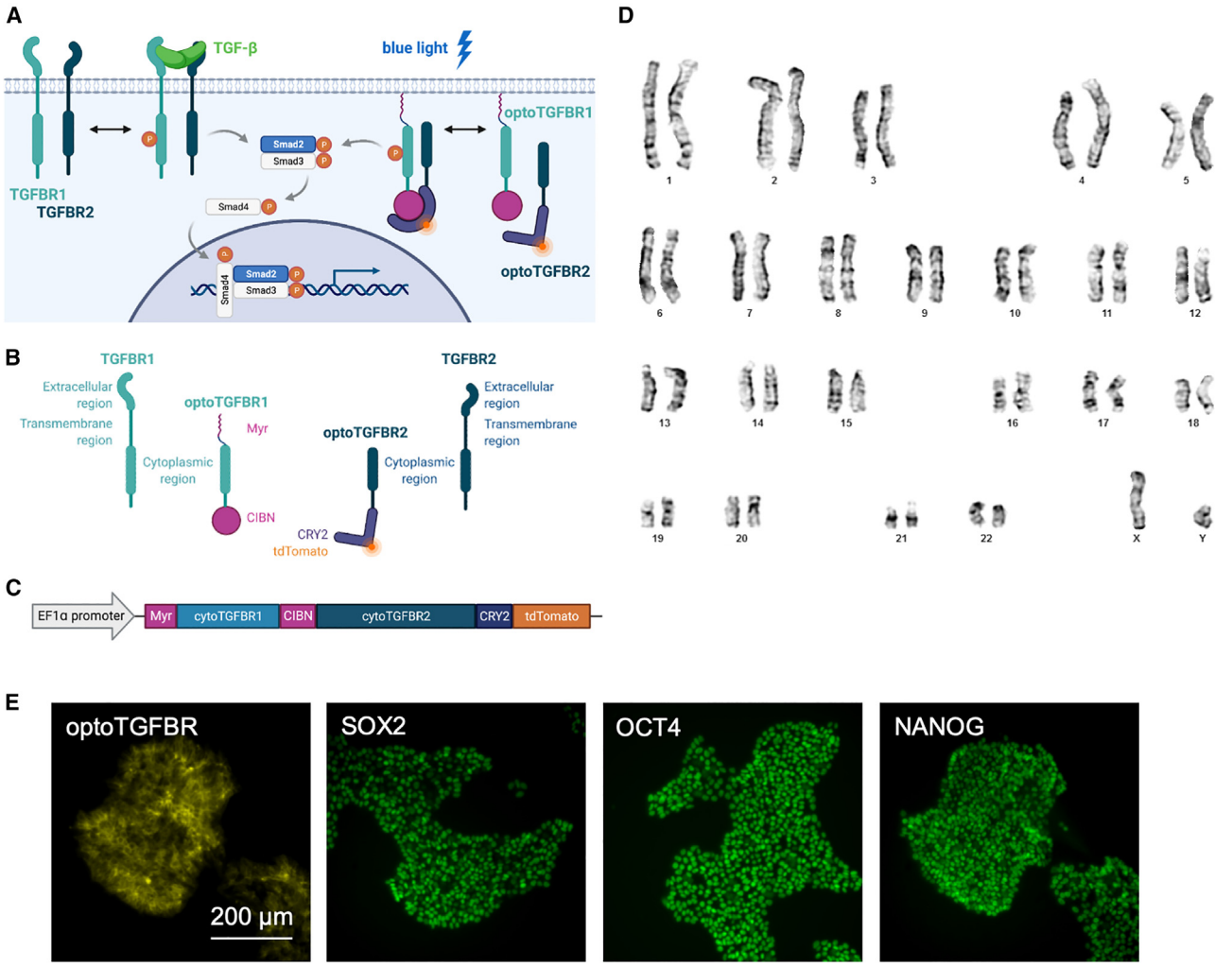

Figure 1. Human induced pluripotent stem cell (hiPSC)-based system for optogenetic TGF-β signaling

(A) Canonical TGF-β signaling pathway via soluble factor-activated endogenous TGF-β receptors (TGFBRs) or blue light-activated optogenetic (opto) TGFBRs.

(B) Endogenous TGFBRs and optoTGFBRs share the same cytoplasmic regions.

(C) Lentiviral vector containing optoTGFBRs. Detailed map in Figure S1.

(D) Karyotype of optogenetic hiPSCs.

(E) tdTomato-tagged optoTGFBRs and immunofluorescently stained pluripotency markers in clonal population of optogenetic hiPSCs. Scale bar, 200 μm. Additional characterization displayed in Figure S2.

receptors, with over 70% tdTomato-positive cells as quantified by flow cytometry (Figure 2A). Further flow analysis showed high expression of mesenchymal markers CD73, CD90, and CD105 with low expression of lineage markers CD45 (leukocytes), CD34 (hematopoietic progenitors, endothelial cells), CD14 (monocytes, macrophages), CD79a (B cells), HLA-DR (human antigen-presenting cells, interferon gamma-stimulated MSCs), gated based on isotype controls (Figure 2B). Importantly, mesenchymal cell surface marker expression was similar between optogenetic and non-optogenetic hiMSCs. Both cell populations had a different CD105 profile than human bone marrow-derived MSCs (Figure S3).

Compared with wild-type hiPSC-derived MSCs, optohiMSCs demonstrated similar capacity for tri-differentiation into adipogenic, osteogenic, and chondrogenic lineages, as evidenced by immunostaining for respective markers of fatty acid binding protein 4 (FABP4), alkaline phosphatase (ALP), and aggrecan (Figure S4A). These data satisfy the criteria for validating the MSC phenotype.[25] Using an antibody recognizing the extracellular region of TGFBR1, a region that was not included in optoTGFBR1, western blotting showed similar expression levels of the soluble factor-activated endogenous receptors in non-optogenetic and optogenetic hiMSCs (Figure S4B).

Without light activation, optoTGFBR1 was tethered to the plasma membrane, while optoTGFBR2, and thus the tdTomato fluorescent signal, were diffuse in the cytoplasm (Figure 2C). Upon activation with blue light, the interaction between optoTGFBRs resulted in recruitment of optoTGFBR2 to the plasma membrane, with a localized increase in tdTomato signal that was

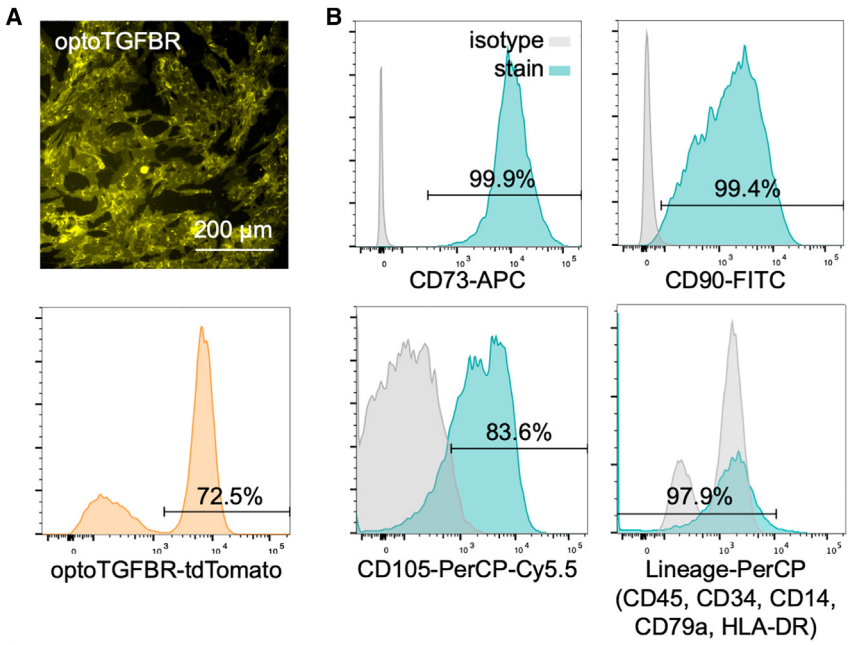

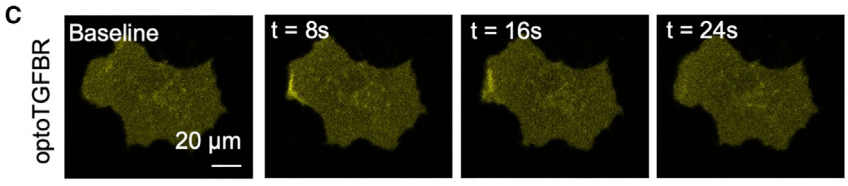

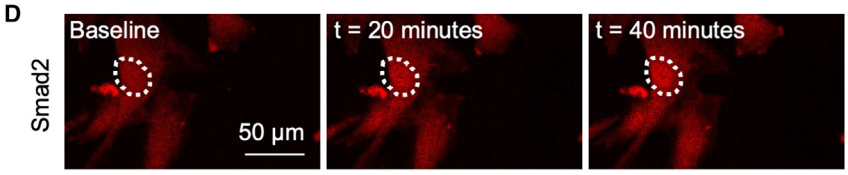

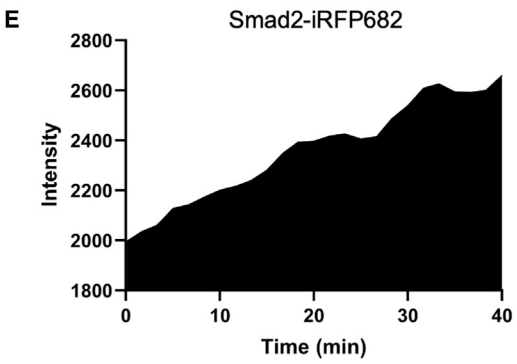

Figure 2. Characterization of optohiPSC-derived mesenchymal stem cells (optohiMSCs)

(A) optohiMSC morphology on standard tissue culture plastic and tdTomato-optoTGFBR expression. Scale bar, 200 μm.

(B) Flow analysis for mesenchymal CD73, CD90, CD105, and lineage markers (CD45, CD34, CD14, CD79a, HLA-DR). Additional characterization displayed in Figures S3 and S4.

(C) Plasma membrane localization of tdTomato-optoTGFBR2. Left: baseline, after 3 min of imaging without stimulation. Middle left: following a 1 s pulse of 488 nm confocal laser, response after 8 s; middle right: 16 s; right: 24 s. Scale bar, 20 μm.

(D) Nuclear localization of iRFP682-tagged Smad2. Left: baseline, after 3 min of imaging without stimulation. Middle: following repeated cycles of 488 nm confocal laser stimulation (15 s) and imaging (30 s), response after 20 min; right: 40 min. Scale bar, 50 μm.

(E) Mean intensity of nuclear iRFP682-Smad2 fluorescent signal within the dotted areas marked in (D). See also Video S1.

initially observed. The optoTGFBRs subsequently dissociated and tdTomato signal dissipated approximately 30 s after initial activation, similar to prior reports for an immortalized cancer cell line.[24] The downstream response of light-activated TGF-β signaling was expected to be the same as ligand-activated canonical signaling with respect to Smad phosphorylation and nuclear localization. In optohiMSCs transduced with iRFP682-tagged Smad2, nuclear translocation was observable about 20 min after light stimulation, with a stronger nuclear signal by 40 min (Figures 2D and 2E). These data are consistent with the published work on the temporal dynamics of TGF-β signaling initiated by the optoTGFBRs.[24]

Derivation of the smooth muscle lineage from optohiMSCs

To demonstrate that light could be used to drive cell differentiation beyond upstream TGF-β signaling pathway responses such as receptor clustering or nuclear localization of the Smad complex, we first used our optogenetic TGF-β system to recapitulate smooth muscle differentiation.[8] It is known that TGF-β/Smad2 signaling induces the differentiation of MSCs into smooth muscle cells *in vitro*.[28]

Monolayers of optohiMSCs were allowed to reach 70%–80% confluency in black-walled, cover glass-bottomed 24-well plates before they were switched to basal smooth muscle induction medium consisting of high glucose DMEM (hgDMEM), low fetal bovine serum (FBS; 5%), and penicillin-streptomycin (P/S; 1%), with no soluble TGF-β or optogenetic stimulation, with soluble TGF-β3 alone (10 ng/mL), or with 488 nm optogenetic stimulation alone (3 or 6 μW/1.9 cm^2, 5 min pulses every 2 h) over 2 weeks of culture (Figure 3A). We verified with a HEK293 cell-based reporter assay that the serum did not contain detectable levels of TGF-β (Figure S5).

Based on reported designs,[29] we built a light stimulation device compatible with long-term incubator culture, readily

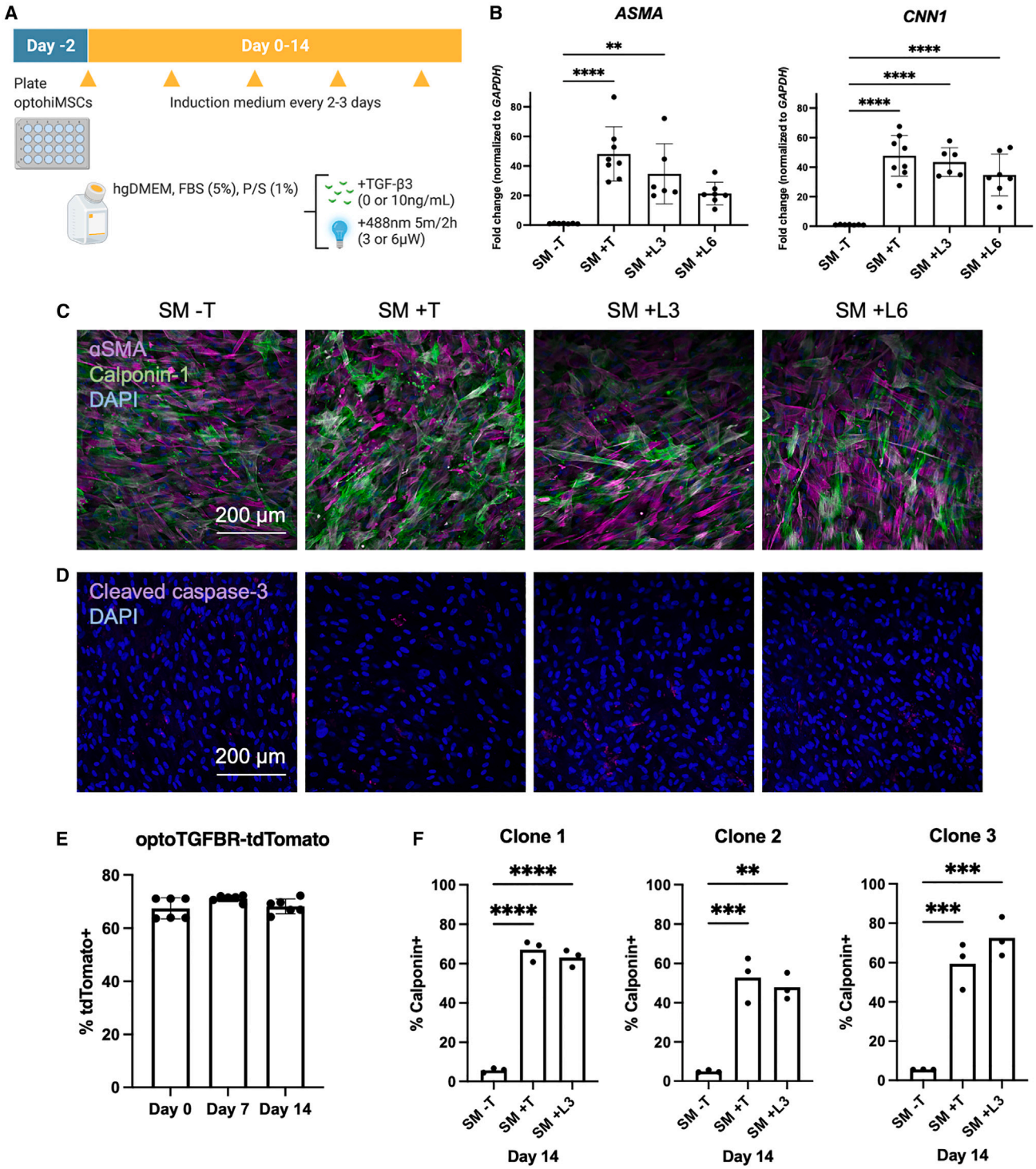

Figure 3. TGF-β-mediated smooth muscle differentiation

(A) optohiMSCs were plated in monolayers on black-walled 24-well plates and allowed to reach 70%–80% confluency over 2 days. They were then switched to basal smooth muscle medium (SM) with no TGF-β (−T), 10 ng/mL TGF-β3 (+T), or 3 or 6 μW 488 nm light with 5 min pulses every 2 h (+L3, +L6) for 14 days total.

(B) qRT-PCR for α smooth muscle actin (*ASMA*) and calponin-1 (*CNN1*).

(C) Immunofluorescent staining for *ASMA* (purple), *CNN1* (green), and DAPI (blue). Scale bar, 200 μm.

(D) Immunofluorescent staining for cleaved caspase-3 (purple) and DAPI (blue). Scale bar, 200 μm.

(E) Flow cytometry analysis for optoTGFBR-tdTomato expression over the course of smooth muscle differentiation.

(legend continued on next page)

adaptable for any well plate format, consisting of 192 individually programmable blue LEDs, with limited spillover between wells to allow for parallel experiments. The light-stimulation regimen (intensity and timing of light exposure) was selected to drive differentiations while minimizing potential phototoxic effects.[20,21,24] On the light-stimulation device, the 3 μW/well group could be calibrated at 3 ± 1 μW, and the 6 μW/well group could be calibrated at 6 ± 0.6 μW (Figure S6).

Contractile proteins such as α smooth muscle actin and calponin-1 are commonly used to assess the smooth muscle cell phenotype.[28] Expression of smooth muscle differentiation markers was evaluated by qRT-PCR, immunostaining, and flow cytometry at day 14. Gene expression of α smooth muscle actin (*ASMA*) normalized to *GAPDH* was significantly upregulated in groups that had received either soluble TGF-β (48-fold, $p < 0.0001$) or optogenetic stimulation of TGF-β at 3 μW/well (35-fold, $p < 0.01$) compared with the group that received no stimulation (Figure 3B). *ASMA* expression was also elevated in the group that received optogenetic stimulation at 6 μW/well (21-fold). In all TGF-β-stimulated groups, calponin-1 (*CNN1*) mRNA expression was significantly upregulated (+T 36-fold, +L3 43-fold, +L6 35-fold; all $p < 0.0001$) compared with the negative control (Figure 3B). These results were corroborated by immunostaining for the same markers (Figure 3C). Additional immunostaining for apoptosis marker cleaved caspase-3 showed minimal phototoxicity after 2 weeks of optogenetic stimulation (Figure 3D). Flow analysis for tdTomato expression indicated no loss of optoTGFBR expression throughout the 2 week differentiation period (Figure 3E). Across three clonally derived optohiMSC populations, quantitative flow analysis for calponin showed significantly elevated expression in both TGF-β-treated groups (clone 1: 67%, $p < 0.0001$; clone 2: 53%, $p < 0.001$; clone 3: 59%, $p < 0.001$) and light-treated groups (clone 1: 64%, $p < 0.0001$; clone 2: 46.3%, $p < 0.01$; clone 3: 73%, $p < 0.001$) compared with the control group (Figure 3F).

Derivation of the tenogenic lineage from optohiMSCs

TGF-β is a critical factor in the tenogenic differentiation of MSCs, with high potency of TGF-β alone and enhanced effects when applied in combination with other growth factors.[9,30] We sought to recapitulate the tenogenic differentiation of MSCs using light stimulation following stepwise supplementation with other tenogenic factors and TGF-β. We used the same basal medium consisting of hgDMEM, FBS (5%), and P/S (1%) but supplemented it with ascorbic acid (50 μg/mL), growth/differentiation factor-7 (GDF-7/BMP-12; 100 ng/mL), and, after 3 days, connective tissue growth factor (CTGF; 100 ng/mL).[9] Monolayers of optohiMSCs were plated on 24-well plates, and groups received no soluble TGF-β or optogenetic stimulation, soluble TGF-β3 alone (10 ng/mL), or optogenetic stimulation alone (3 or 6 μW/1.9 cm^2, 5 min pulses every 2 h) over 2 weeks total (Figure 4A).

Similarly, we evaluated gene and protein expression of tenogenic markers after 14 days of differentiation. Scleraxis, a transcription factor known to be activated by TGF-β in MSCs in tenogenesis, can serve as an early marker of tendon progenitors throughout tendon development.[31] Compared with the group that had neither endogenous nor optogenetic TGF-β signaling activated, gene expression of scleraxis (*SCX*) normalized to *GAPDH* was upregulated in all groups (+T 18-fold, +L3 8-fold, +L6 6-fold) and most significantly in soluble TGF-β and 3 μW/well conditions (+T $p < 0.0001$, +L3 $p < 0.05$) (Figure 4B). Gene expression levels of collagen I (*COL1A1*) normalized to *GAPDH* were significantly increased in all groups that had TGF-β signaling activated by soluble factor (+T 5-fold, +L3 4-fold, +L6 3-fold; all $p < 0.0001$) over the negative control (Figure 4B), suggesting maturation of tendon matrix.[31] Immunostaining for *SCX* and collagen I showed similar trends consistent with the qRT-PCR data (Figure 4C).

Derivation of the chondrogenic lineage from optohiMSCs

In MSC-based cartilage tissue engineering, TGF-β is one of the most widely used mediators to drive chondrogenesis and promote tissue growth, acting through SRY-box transcription factor 9 (SOX9).[3] It is also known that chondrogenic potential is greatly enhanced under 3D culture settings.[26] Thus, for chondrogenic studies of optogenetically activated TGF-β signaling, optohiMSCs were encapsulated in hydrogel (20 million cells/mL 2% agarose hydrogel; Figure 5A). The hydrogel discs were 6 mm in diameter and 1.5 mm thick to fit into the 96-well plate format of the optogenetic stimulation device.

Two days following encapsulation, the hydrogels were switched to chondrogenic medium consisting of hgDMEM, P/S (1%), insulin-transferrin-selenium mix (1%), HEPES (10 mM), sodium pyruvate (0.9 mM), dexamethasone (100 nM), L-proline (50 μg/mL), and ascorbic acid (50 μg/mL).[4] Groups received no soluble TGF-β or optogenetic stimulation, soluble TGF-β3 alone (10 ng/mL), or optogenetic stimulation alone (3 or 6 μW/0.32 cm^2, 5 min pulses every 2 h) over 3 weeks of culture (Figure 5B).

After 21 days of differentiation, we performed global quantitative proteomics on samples from two independent experiments, with n = 3 replicates per group. A heatmap with hierarchical clustering of samples based on relative protein expression was generated. At the highest level, samples from the same experiment were more related to each other than to samples from another experiment (Figure 5C). Within both experiments, groups that received optogenetic stimulation (+L3, +L6) had protein expression profiles more similar to those in the soluble TGF-β3-treated positive control group (+T) than to the untreated negative control group that received neither soluble factor nor optogenetic TGF-β stimulation (−T), though the light-stimulated groups had expression profiles more similar to each other than the soluble TGF-β3-treated group.

Comparing the positive and negative control groups (+T/−T), we identified significantly changed proteins with the absolute log_2 fold change (FC) >0.58 and false discovery rate Q <0.05 (Figure 5D). As

(F) Flow cytometry analysis for calponin expression in three clonal optohiMSC populations.

All data represent means ± SD with n ≥ 6 in (B), n = 6 in (E), and n = 3 in (F). **p < 0.01, ***p < 0.001, ****p < 0.0001 as calculated by one-way analysis of variance (ANOVA) and post hoc Tukey-Kramer's multiple comparisons test, except for qPCR of *ASMA* in (B), which was calculated by Kruskal-Wallis and post hoc Dunn's multiple comparisons test.

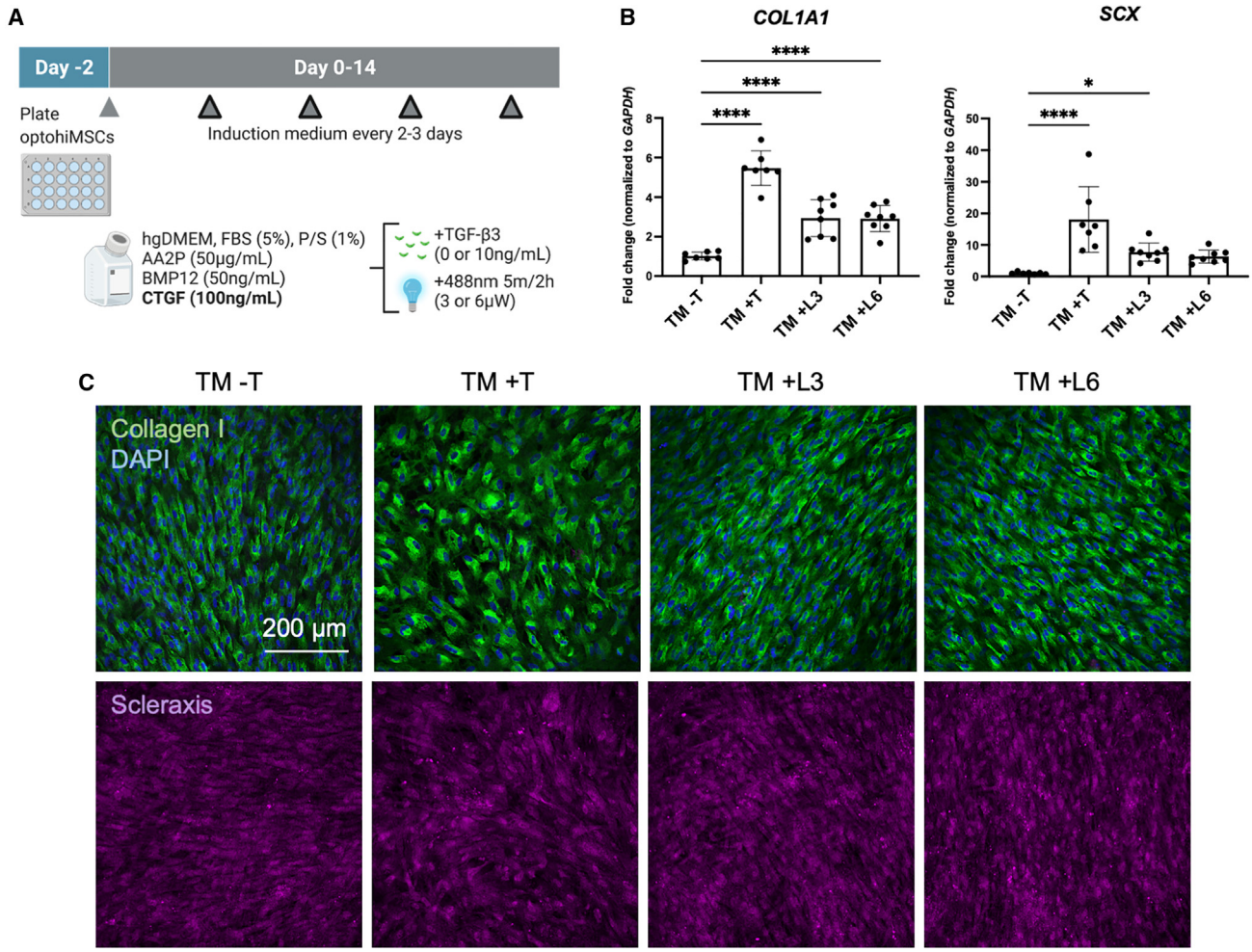

Figure 4. TGF-β-mediated tenogenic differentiation

(A) optohiMSCs were plated in monolayers on black-walled 24-well plates and allowed to reach 70%–80% confluency over 2 days. They were then switched to basal tenogenic medium (TM) with no TGF-β (−T), 10 ng/mL TGF-β3 (+T), or 3 or 6 μW 488 nm light with 5 min pulses every 2 h (+L3, +L6) for 14 days total.

(B) qRT-PCR for collagen I (*COL1A1*) and scleraxis (*SCX*).

(C) Immunofluorescent staining for *COL1A1* (green), DAPI (blue), and *SCX* (purple). Scale bar, 200 μm.

All data represent means ± SD with n ≥ 7 in (B). *p < 0.05, ****p < 0.0001 as calculated by one-way ANOVA and post hoc Tukey-Kramer's multiple comparisons test.

expected, significantly increased protein expression of TGF-β3 was detected in the soluble factor-treated group (+T), with a $\log_2$FC >2 compared with all other groups (−T, +L3, +L6).

Compared with the untreated group (−T), all soluble TGF-β- and light-stimulated groups (+T, +L3, +L6) had significantly upregulated expression of calcium/calmodulin-dependent protein kinase kinase 1 (CAMKK1). CAMKK1 has been linked to pathways including sulfation of chondroitin, cartilage formation, and TGF-β signaling, and it is thought to be upregulated when the highly anti-chondrogenic hsa-miR-221 is inhibited.[32]

Compared with the untreated group (−T), the soluble TGF-β- and 3 μW light-treated groups (+T, +L3) had significantly upregulated expression of protein mago nashi homolog (MAGOH), one of the three core components in the exon junction complex interacting with SOX9, a critical transcription factor for cartilage development and homeostasis.[33] Studies have also shown that knockdown of MAGOH had similar effects on gene splicing as depletion of SOX9 itself.[34] Matrix metalloproteinase 23 (MMP23B), another significantly upregulated protein in 10 ng/mL TGF-β3- and 3 μW light-treated samples (+T, +L3), has been linked to cartilage or bone formation and metabolism. In a murine model, *Mmp23* gene expression in chondrocytes and osteoblasts exhibited time-dependent changes similar to collagen II expression profiles, with a suggested role in endochondral ossification.[35]

Cartilage-bone tissue model of optogenetic stimulation

It has been established that both spatiotemporal gradients of TGF-β signaling and bone substrate for cartilage formation support the development of stratified cartilage.[4,36,37] However, it was not possible to simultaneously leverage these findings in a single engineered system. Using optohiMSCs, we formed chondrogenic spheroids and fused them into a cohesive and cell-dense layer of

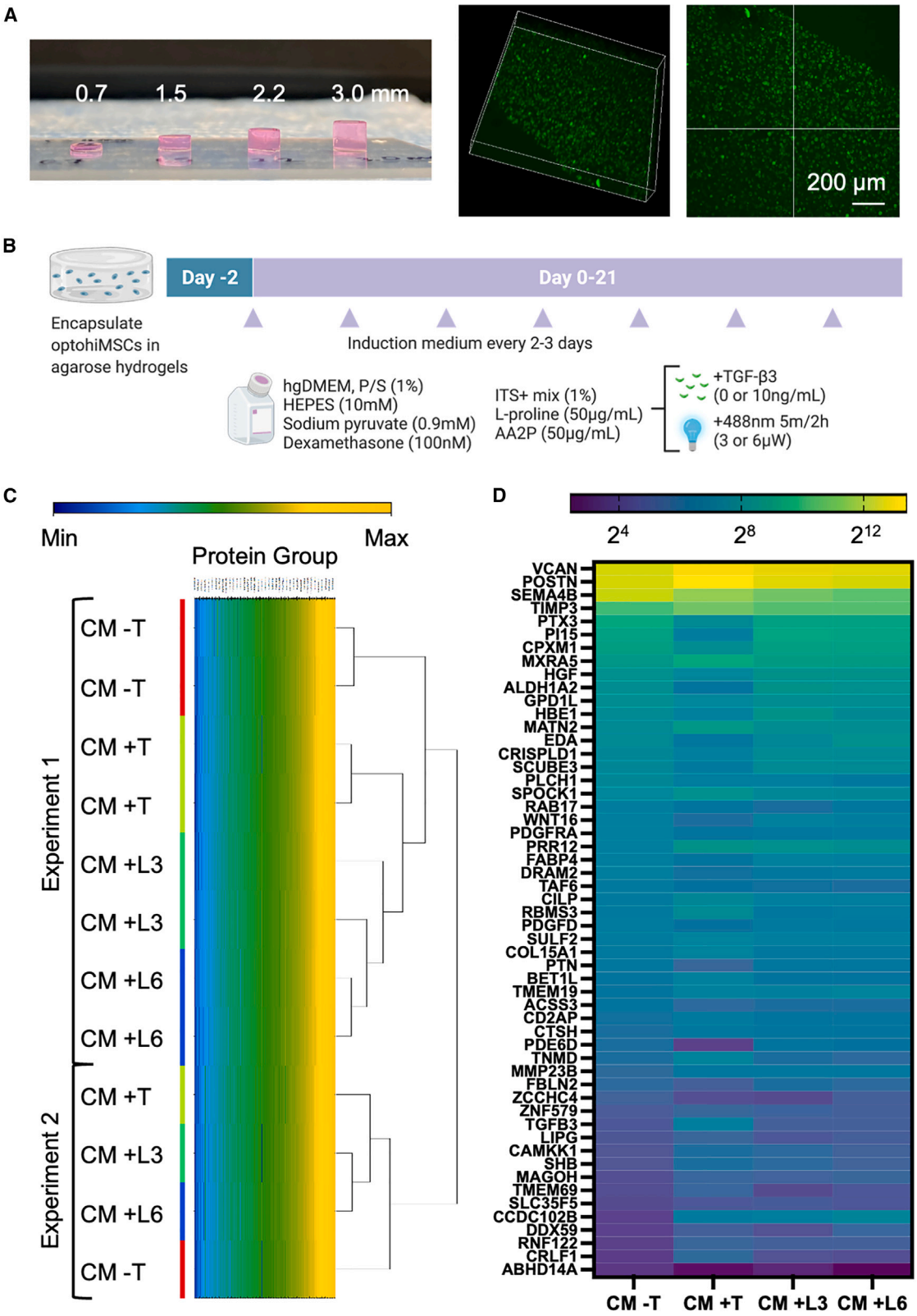

(legend on next page)

cartilage integrated with a subchondral bone scaffold. After an initial 3 week period of isotropic chondrogenic induction using 10 ng/mL soluble TGF-β, optogenetically activated TGF-β signaling induced the formation of hyaline cartilage at the surface while attenuating with depth to enable hypertrophic induction at the osteochondral interface. For the subsequent 6 weeks, tissues were distributed among groups that (1) had TGF-β3 withdrawn for the remainder of culture, (2) continued to be supplemented with soluble TGF-β3, or (3) had TGF-β3 withdrawn but received optogenetic stimulation instead (Figure 6A). The optogenetic stimulation regimen consisted of 5 min pulses every 2 h at 3 μW intensity over the 1.9 cm^2 area of a 24-well plate, with the superficial surface of the cartilage forming proximal to the 488 nm light source.

Second harmonic generation (SHG) imaging revealed the extent of collagen fibrillar organization (Figure 6B). The SHG signal scaled to the fibril thickness squared.[38] Collagen I, a dominant component in bone matrix, typically forms thicker fibrils than collagen II, the primary form of cartilage collagen. In the tissues that had TGF-β signaling activated by soluble factor or light stimulation, fibrils running parallel to the articular surface were found in the superficial region. Tissues that received no TGF-β stimulation after 3 weeks had some of these parallel fibrils, though with a faint SHG signal or lacking continuity across the superficial surface.

Staining for cartilage markers aggrecan and lubricin was performed on sections across the tissue depth. In tissues that continued to receive TGF-β stimulation by either soluble factor or light, aggrecan and clusterin stained more strongly overall than in tissues that had TGF-β withdrawn after the initial 3 weeks (Figure 6C). In the optogenetically treated group, aggrecan and clusterin expression appeared more concentrated at the superficial surface of the cartilage compared with the soluble TGF-β3-treated group, in which there was no depth-dependent pattern of expression.

Selective differentiation of optohiMSCs in co-culture

To demonstrate an advantage of using the optogenetic system rather than soluble factors to manipulate TGF-β signaling, non-optogenetic and optogenetic hiMSCs were sorted for MSC marker CD90, then mixed at a 2:1 ratio in co-culture and maintained using shared culture medium comprised of hgDMEM, FBS (5%), and P/S (1%) (Figures 7A and 7B). The goal was to show the ability to simultaneously maintain both a stromal/stem-like population as well as a differentiated smooth muscle-like population in a single culture.

Using calponin-1 as a marker of smooth muscle cell phenotype, as before,[28] all populations showed increased expression after 2 weeks in co-culture (Figures 7C and 7D). Calponin expression in non-optogenetic hiMSCs (tdTomato−) from the soluble TGF-β3-treated co-cultures was significantly higher (61.4%) than the counterparts in blue light-treated co-cultures (42.4%, $p < 0.01$) (Figure 7C). In the light-responsive hiMSC population (tdTomato+), both soluble factor- and blue light-treated groups had calponin expression significantly higher than the negative control (10.9%, $p < 0.0001$), with no significant difference from one other (+T 85.4%, +L3 85.7%) (Figure 7D).

DISCUSSION

We report the development of an optogenetic hiPSC system with demonstrated utility to control and study TGF-β signaling during differentiation into MSCs and subsequently into smooth muscle cells, tenocytes, and chondrocytes. Optogenetic stimulation of TGF-β expression in the absence of its soluble form was observed to upregulate gene and protein expression of known markers for directed differentiation of hiPSCs into mesenchymal lineages (smooth muscle cells, tenocytes, and chondrocytes), with only minimal phototoxicity over multiple weeks of culture. Chondrogenic differentiation necessitated cell encapsulation into a thin hydrogel instead of a monolayer culture. We believe that this is the first research article reporting optogenetic-mediated cell differentiation carried out in 3D.[22]

Since its initial applications in neuroscience for precise activation of neural circuits, optogenetics has been recognized for its potential to interrogate cell signaling pathways with fine spatiotemporal control. Such systems, including those developed for Ras/Erk, FGF, Wnt, and BMP signaling,[20,21,39,40] commonly rely on light-activated interactions between optogenetic proteins coupled to signaling receptors. Their characterization has largely been focused on upstream responses such as receptor localization and protein phosphorylation in immortalized cell lines. Only recently have these systems been studied in human adult neural stem cells[41] and human embryonic stem cells (hESCs).[42]

The field has also begun to successfully exploit the temporal advantage of optogenetic tools, delivering a transient pulse of Wnt-activating light for initial hESC mesoderm induction toward differentiation into cardiomyocytes.[42] Another key advantage of optogenetic systems is in the precise spatial patterning of stem cell fate that recapitulates those seen during tissue development and regeneration. The feasibility of applying photomasks or guiding lasers to achieve illumination patterns in optogenetic systems has been demonstrated for cell monolayers.[24,42] Small light-sensitive neural spheroids have been used to pace neuromuscular junctions and cardiac cells.[43–45]

We opted to develop an hiPSC-based optogenetic TGF-β system, as it offers several advantages over other cell types. hiPSCs can be derived from a small sample of blood and expanded near indefinitely, allowing for multiple cell types with or without optogenetic capabilities to be generated from the same source, thus enabling patient-specific studies. However, the introduction of optogenetic systems into hiPSCs may present concerns such

Figure 5. TGF-β-mediated chondrogenic differentiation

(A) optohiMSCs were encapsulated in 2% agarose at 20 × 10^6 cells/mL. Hydrogels can be made to varying thicknesses and cut by biopsy punches to fit a 96-well plate format. Scale bar, 200 μm.

(B) 2 days after encapsulation, 1.5-mm-thick hydrogels were switched to basal chondrogenic medium (CM) with no TGF-β (−T), 10 ng/mL TGF-β3 (+T), or 3 or 6 μW 488 nm light with 5 min pulses every 2 h (+L3, +L6) for 21 days total.

(C) Clustered heatmap showing total protein expression levels.

(D) Candidates with log_2FC 0.58 with false discovery rate (FDR) 0.05 between +T/−T groups, displayed as log_2(mean) of n = 3.

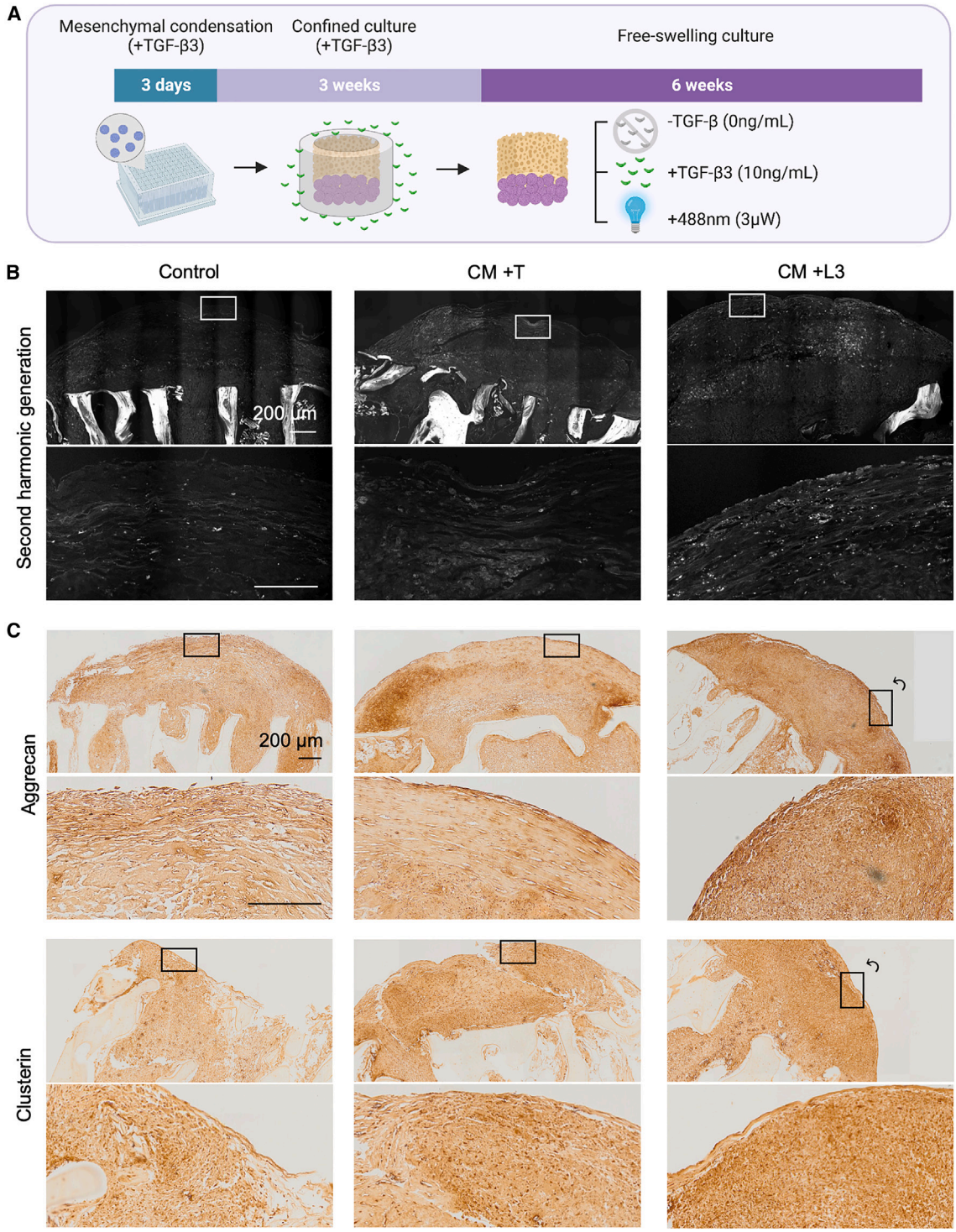

Figure 6. Cartilage-bone tissue model for optogenetic stimulation

(A) optohiMSC-derived chondrogenic spheroids were fused and integrated with a subchondral bone scaffold, maintained under confined culture conditions in complete CM with 10 ng/mL TGF-β3 for 3 weeks, then switched to free-swelling culture conditions in basal CM stimulated with either 10 ng/mL TGF-β3 (+T) or 3 μW 488 nm light with 5 min pulses every 2 h (+L3). Details of cartilage-bone tissue formation are shown in Figure S7.

(B and C) After 6 weeks, tissues were subjected to (B) second harmonic generation imaging for collagen fibril alignment and (C) immunohistochemistry for aggrecan and clusterin. Scale bars, 200 μm.

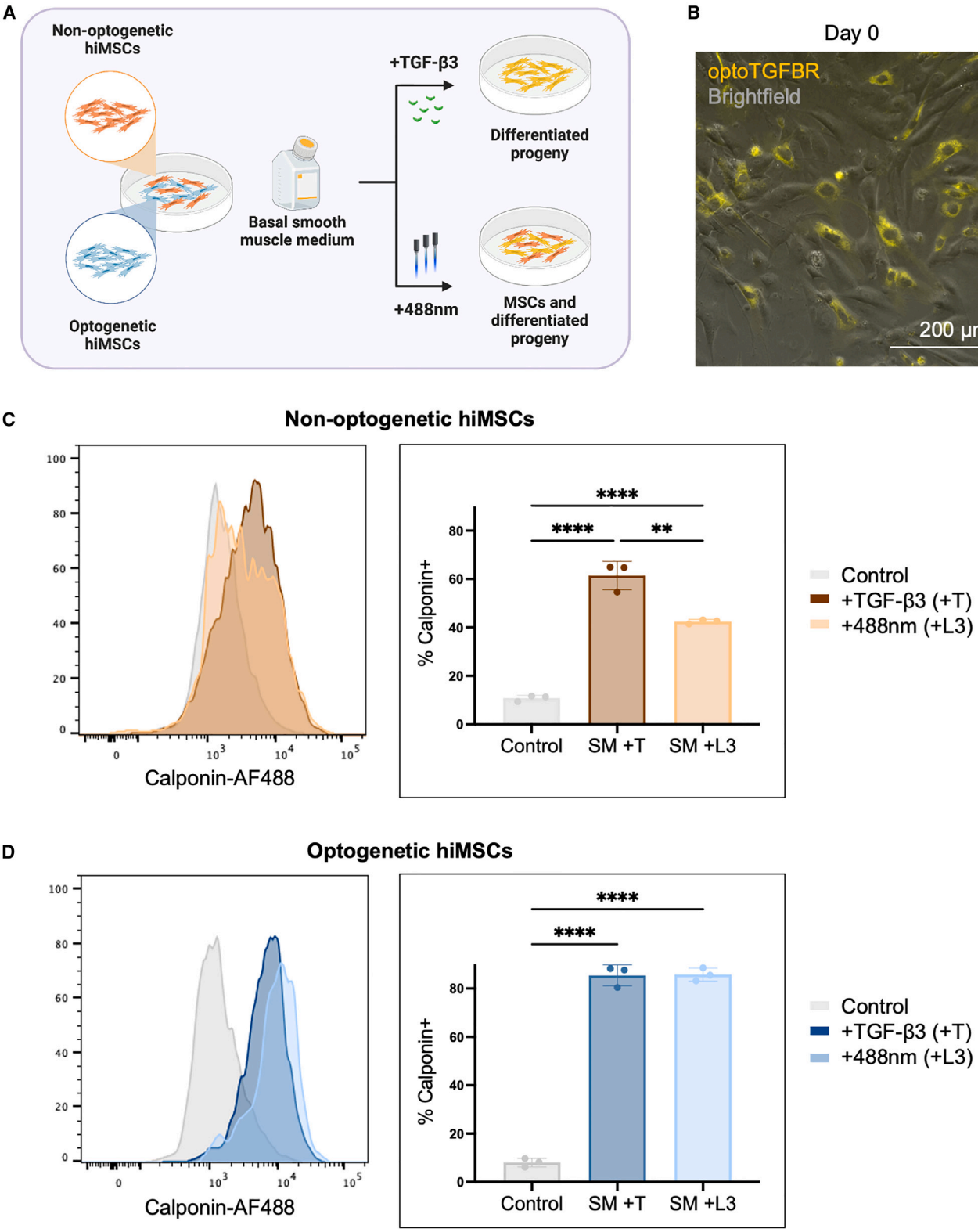

Figure 7. Co-culture of non-optogenetic and optogenetic hiMSCs

(A) Co-cultures of CD90-sorted non-optogenetic and optogenetic hiMSCs were maintained in shared smooth muscle induction medium and stimulated with either 10 ng/mL TGF-β3 (+T) or 3 μW 488 nm light with 5 min pulses every 2 h (+L3) for 2 weeks total.

(legend continued on next page)

as undefined integration with oncogenes or key genes, unstable transient expression, and suppression of endogenous receptors. To mitigate these effects, we opted for a lentiviral delivery approach using the EF-1α promoter, which has shown comparatively high transduction efficiency with low gene silencing and low oncogenic potential.[27] In multiple clones, we confirmed that the transduction protocol we used did not affect the pluripotency of hiPSCs (Figures 1E and S2) or their functional ability to differentiate into hiMSCs (Figures 2B and S3). The remaining assays and experiments were therefore conducted using one clone. We verified a normal karyotype (Figure 1D) and similar expression of endogenous TGFBRs between optogenetic cells and their wild-type counterparts (Figure S4B).

Previous studies of similar optogenetic systems have observed a dose-dependent response to light intensity at the level of protein phosphorylation and a threshold effect of light duration.[20,21,24] Compared with the long-term optogenetic FGF signaling for maintaining stem cell pluripotency (delivering blue light at 1 μW/mm^2 in 1–10 min pulses every 2 h, over several weeks to months),[20] we used 32- and 63-fold lower light intensities with similar timing for our studies and observed no light-induced apoptotic effects over 2 weeks of stimulation of cells cultured in monolayers (Figure 3D).

TGF-β modulates key functions of MSCs ranging from proliferation to multilineage differentiations.[2] Beyond upstream effects in canonical TGF-β signaling such as nuclear localization of the phosphorylated Smad complex, we demonstrated that light-activated TGF-β signaling could drive differentiations into mesenchymal lineages. In our study, expression of the optogenetic system was retained after differentiation (Figures 2A and 3E), and optogenetic editing did not affect the ability of hiPSCs to differentiate into MSCs and downstream progeny (Figure S4A). In smooth muscle differentiation of MSCs, stiff substrate and TGF-β have been identified as critical factors,[8,28] while in tenogenic protocols, stepwise supplementation with additional growth factors is necessary.[9] In medium containing low serum and no TGF-β, we used light-activated TGF-β signaling to recapitulate the role of soluble TGF-β in differentiations of optohiMSCs into smooth muscle and tenogenic lineages (Figures 3A, 4A, and S5). Immunostaining for smooth muscle and tenogenic differentiation markers (Figures 3C and 4C) showed morphological changes comparable to published effects of soluble TGF-β on differentiation into smooth muscle and tenogenic cells.[8,9] In three clonally derived optohiMSC populations, expression of smooth muscle differentiation marker calponin was significantly higher in both TGF-β- and light-stimulated groups compared with the control group (Figure 3F). Based on the expression of these markers after 14 days of differentiation measured in these studies, it will be interesting for future studies to track temporal changes of key transcription factors for each cell lineage throughout the course of differentiation.

We also drove chondrogenic differentiation of optohiMSCs encapsulated in biologically inert 3D agarose hydrogels using chemically defined medium with blue light in lieu of soluble TGF-β3 (Figures 5A and 5B). Our hydrogel-encapsulated optohiMSC model for chondrogenic differentiation demonstrates that optogenetic stimulation can be used in millimeter-sized 3D settings. The 1.5-mm-thick hydrogel discs had the thickness of native human cartilage, serving as a proof of concept for a step toward extending the potential of optogenetic tools into tissue engineering with spatially precise control of cell fate. For optical stimulation through thicker and less translucent tissues, blue light-activated optogenetic tools may be used in conjunction with 2-photon excitation or photon upconversion biomaterials[46–49] or with recently reported red or far-red optogenetic proteins.[39,50–54]

We subsequently incorporated optohiMSC-derived chondrogenic spheroids into the cartilage-bone model, using light-patterned gradients to maintain TGF-β signaling at the articular surface in support of cartilage superficial zone formation (Figure 6). We previously demonstrated using non-optogenetic methods that these gradients resulted in zonal stratification, but it was not possible to interface the engineered cartilage with bone while also manipulating the distribution of soluble factors.[4] To further demonstrate the advantage of an optogenetic system over soluble factor stimulation, we showed the ability to maintain both MSCs and differentiated progeny in the same culture by selective activation of TGF-β signaling (Figure 7). In conjunction with 3D bioprinting or other tools for cell patterning, light-responsive and non-responsive cells can be deposited into prespecified locations to allow for selective stimulation and differentiation. The simultaneous maintenance of stromal support cells and their differentiated progeny could be useful for studying biological scenarios such as the plasticity of MSC-like pericyte vascular support cells to differentiate into vascular smooth muscle cells in arteriogenesis[55,56] or MSC recruitment to sites of bone injury to replace damaged osteoblasts.[57,58]

Across the three mesenchymal lineages studied, groups that received light-activated TGF-β signaling (+L3, +L6) had expression levels of differentiation markers closer to the soluble factor-treated conditions (+T) than to the untreated controls (−T), though at slightly lower expression levels than the soluble TGF-β3-positive control (Figures 3B, 3C, 4B, 4C, 5C, and 5D). We observed this pattern across multiple assays including qRT-PCR, immunostaining, and global quantitative proteomics. Interestingly, effects of 5 min pulses of blue light every 2 h in the 3 μW light-treated groups (+L3) were more similar to conventional soluble TGF-β3-treated groups (+T) than the same regime in the 6 μW light-treated groups (+L6). An increase in the intensity of optogenetic stimulation did not result in upregulation of differentiation markers, suggesting the need for further optimization of

(B) Bright-field image with fluorescence overlay showing non-optogenetic (tdTomato−) and optogenetic (tdTomato+) hiMSCs prior to smooth muscle induction and TGF-β stimulation. Scale bar, 200 μm.
(C) Flow cytometry analysis for calponin expression in non-optogenetic hiMSC population.
(D) Flow cytometry analysis for calponin expression in optogenetic hiMSC population.
All data represent means ± SD (n = 3). **p < 0.01, ****p < 0.0001 as calculated by one-way ANOVA and post hoc Tukey-Kramer's multiple comparisons test.

illumination conditions with additional parameters such as pulse length or frequency.

One limitation of this study is that hiPSC-derived cells do not fully recapitulate the function or phenotype of primary cells from adult tissues, which is well known in the field.[59–61] We observed differences in MSC surface marker expression between bone marrow and iPSC-derived MSCs (Figure S3), consistent with previous reports that hiMSCs have gene expression profiles reminiscent of vascular progenitor cells.[59] However, with the increasing success in maturing hiPSC derivatives, these cells continue to serve as an attractive cell source in areas ranging from patient-specific *in vitro* models for drug screening and disease modeling to personalized cell therapies for regenerative medicine.

The precise spatiotemporal control of TGF-β signaling by optogenetic tools provide opportunities for a more comprehensive understanding of hiPSC behavior and the development of hiPSC-specific differentiation protocols. We and others have opted for lentiviral delivery of optogenetic systems,[21,39–41] but with the recent rise of CRISPR-Cas9 technologies, highly specific knockins to prescribed safe harbor loci are increasingly used.[20,42] Improvements in genetic modification techniques will increase the ease with which complex optogenetic systems can be delivered, though adeno-associated viral (AAV) vectors have successfully been used to transduce cells *in vivo* for clinical optogenetic applications, notably for the partial restoration of visual function in a human patient.[62,63]

The hiPSC-based optogenetic tool described here could also be applied to study the versatile roles of the TGF-β family in the regulation of a number of conditions ranging from fibrosis to inflammation and cancer stemness. For example, there is an opportunity to study the crosstalk between TGF-β signaling and other pathways, such as BMP in a developing joint or Ras/Erk in cancer progression.[64,65] With recent advances in the ease and efficiency of genome editing, it may soon become possible to concurrently express and orthogonally control multiple optogenetic signaling pathways in a single hiPSC line. The necessary optogenetic tools, including multicolor light-responsive proteins and illumination devices, are also under development.[29,39,50–54]

In summary, we demonstrate the capability of a novel hiPSC-based optogenetic system to direct TGF-β-mediated mesenchymal differentiation into smooth muscle, tenogenic, and chondrogenic lineages. The resulting optogenetically edited cells can serve as a versatile tool for regulating TGF-β signaling in MSCs. The collected data suggest that optogenetic regulation of TGF-β signaling can enable precise control of hiPSC differentiation into mesenchymal lineages toward more comprehensive understanding of the role of TGF-β in regulating MSC function. Future work can harness the advantages of an optogenetic tool to study and manipulate TGF-β signaling with unprecedented spatiotemporal control.

Limitations of the study

As detailed above, a limitation of this study is that hiPSC-derived cells do not fully recapitulate the phenotypes of primary cells from adult tissues, which is a known general limitation in the field. Also, the clonal lines of optogenetic hiPSCs were generated in the GM25256 (WTC11) background, a well-characterized healthy male cell line that has been used for studies of many other conditions and diseases.[66–68] Although we confirmed key functionalities in three separate optohiPSC clones—pluripotency following lentiviral transduction of the optogenetic system, expression of mesenchymal cell surface markers following differentiation into optohiMSCs, and differentiation into the smooth muscle lineage—it would be of interest to generate optohiPSC clones from different backgrounds for more extensive validation.

STAR★METHODS

Detailed methods are provided in the online version of this paper and include the following:

- KEY RESOURCES TABLE
- RESOURCE AVAILABILITY
  - Lead contact
  - Materials availability
  - Data and code availability
- EXPERIMENTAL MODEL AND SUBJECT DETAILS
  - Plasmid preparation
  - Lentiviral transduction and stable hiPSC line generation
- METHOD DETAILS
  - hiPSC to MSC differentiation
  - Flow cytometry for MSC cell surface markers
  - Tri-differentiation of MSCs
  - Western Blot for TGFBR
  - Blue light optogenetic stimulation
  - Smooth muscle and tenogenic differentiations
  - Chondrogenic differentiation
  - RNA isolation and qPCR analysis
  - Immunostaining
  - Global quantitative proteomic analysis
  - Cartilage-bone tissue formation
  - Second harmonic generation imaging
  - Non-optogenetic and optogenetic hiMSC Co-Culture
- QUANTIFICATION AND STATISTICAL ANALYSIS

SUPPLEMENTAL INFORMATION

Supplemental information can be found online at https://doi.org/10.1016/j.celrep.2023.112509.

ACKNOWLEDGMENTS

We thank Michael Kissner and Daniel Troast at the Columbia Stem Cell Initiative Flow Cytometry Core for lending their expertise to the project. We thank Dr. Sharon Fleischer, Dr. Pamela Graney, Dr. Carla Huerta-López, Dr. Andy J. Lee, Max Summers, and Dr. Manuel A. Tamargo for their support on this work. Graphical figures were created with BioRender.com. We gratefully acknowledge funding support by the NIH (grants EB027062 and AR078707) and NSF GRFP (grant 1644869). These studies used the resources of the Herbert Irving Comprehensive Cancer Center Confocal and Specialized Microscopy Shared Resource funded in part through the NIH (grant P30CA013696).

AUTHOR CONTRIBUTIONS

J.Y.W., C.T.H., and G.V.-N. designed experiments. J.Y.W. and G.V.-N. wrote the paper. J.Y.W. and K.Y. designed and fabricated light-stimulation devices. R.K.S. performed global quantitative proteomic analysis. J.Y.W. and D.N.T.

performed flow cytometry. J.Y.W., M.M., and B.W. performed western blotting and related data analyses. J.Y.W. conducted all other experiments.

DECLARATION OF INTERESTS

G.V.-N. and K.Y. hold equity in Epibone and are entitled to royalties through Columbia's license to Epibone. G.V.-N. is a member of Epibone's board of directors.

INCLUSION AND DIVERSITY

We support inclusive, diverse, and equitable conduct of research.

Received: June 24, 2022
Revised: December 28, 2022
Accepted: April 28, 2023
Published: May 12, 2023

REFERENCES

1. Mizuguchi, T., and Matsumoto, N. (2007). Recent progress in genetics of Marfan syndrome and Marfan-associated disorders. J. Hum. Genet. *52*, 1–12. https://doi.org/10.1007/s10038-006-0078-1.
2. de Araújo Farias, V., Carrillo-Gálvez, A.B., Martín, F., and Anderson, P. (2018). TGF-β and mesenchymal stromal cells in regenerative medicine, autoimmunity and cancer. Cytokine Growth Factor Rev. *43*, 25–37. https://doi.org/10.1016/j.cytogfr.2018.06.002.
3. Byers, B.A., Mauck, R.L., Chiang, I.E., and Tuan, R.S. (2008). Transient exposure to transforming growth factor beta 3 under serum-free conditions enhances the biomechanical and biochemical maturation of tissue-engineered cartilage. Tissue Eng. *14*, 1821–1834. https://doi.org/10.1089/ten.tea.2007.0222.
4. Ng, J.J., Wei, Y., Zhou, B., Bernhard, J., Robinson, S., Burapachaisri, A., Guo, X.E., and Vunjak-Novakovic, G. (2017). Recapitulation of physiological spatiotemporal signals promotes in vitro formation of phenotypically stable human articular cartilage. Proc. Natl. Acad. Sci. USA *114*, 2556–2561. https://doi.org/10.1073/pnas.1611771114.
5. Albro, M.B., Nims, R.J., Durney, K.M., Cigan, A.D., Shim, J.J., Vunjak-Novakovic, G., Hung, C.T., and Ateshian, G.A. (2016). Heterogeneous engineered cartilage growth results from gradients of media-supplemented active TGF-β and is ameliorated by the alternative supplementation of latent TGF-β. Biomaterials *77*, 173–185. https://doi.org/10.1016/j.biomaterials.2015.10.018.
6. Cigan, A.D., Nims, R.J., Vunjak-Novakovic, G., Hung, C.T., and Ateshian, G.A. (2016). Optimizing nutrient channel spacing and revisiting TGF-beta in large engineered cartilage constructs. J. Biomech. *49*, 2089–2094. https://doi.org/10.1016/j.jbiomech.2016.05.020.
7. Zi, Z., Feng, Z., Chapnick, D.A., Dahl, M., Deng, D., Klipp, E., Moustakas, A., and Liu, X. (2011). Quantitative analysis of transient and sustained transforming growth factor-β signaling dynamics. Mol. Syst. Biol. *7*, 492. https://doi.org/10.1038/msb.2011.22.
8. Park, J.S., Chu, J.S., Tsou, A.D., Diop, R., Tang, Z., Wang, A., and Li, S. (2011). The effect of matrix stiffness on the differentiation of mesenchymal stem cells in response to TGF-β. Biomaterials *32*, 3921–3930. https://doi.org/10.1016/j.biomaterials.2011.02.019.
9. Yin, Z., Guo, J., Wu, T.Y., Chen, X., Xu, L.L., Lin, S.E., Sun, Y.X., Chan, K.-M., Ouyang, H., and Li, G. (2016). Stepwise differentiation of mesenchymal stem cells augments tendon-like tissue formation and defect repair in vivo. Stem Cells Transl. Med. *5*, 1106–1116. https://doi.org/10.5966/sctm.2015-0215.
10. Lotz, S., Goderie, S., Tokas, N., Hirsch, S.E., Ahmad, F., Corneo, B., Le, S., Banerjee, A., Kane, R.S., Stern, J.H., et al. (2013). Sustained levels of FGF2 maintain undifferentiated stem cell cultures with biweekly feeding. PLoS One *8*, e56289. https://doi.org/10.1371/journal.pone.0056289.
11. Onuma, Y., Higuchi, K., Aiki, Y., Shu, Y., Asada, M., Asashima, M., Suzuki, M., Imamura, T., and Ito, Y. (2015). A stable chimeric fibroblast growth factor (FGF) can successfully replace basic FGF in human pluripotent stem cell culture. PLoS One *10*, e0118931. https://doi.org/10.1371/journal.pone.0118931.
12. Ahmadian Baghbaderani, B., Tian, X., Scotty Cadet, J., Shah, K., Walde, A., Tran, H., Kovarcik, D.P., Clarke, D., and Fellner, T. (2016). A newly defined and xeno-free culture medium supports every-other-day medium replacement in the generation and long-term cultivation of human pluripotent stem cells. PLoS One *11*, e0161229. https://doi.org/10.1371/journal.pone.0161229.
13. Stockwell, B.R., and Schreiber, S.L. (1998). Probing the role of homomeric and heteromeric receptor interactions in TGF-β signaling using small molecule dimerizers. Curr. Biol. *8*, 761–770. https://doi.org/10.1016/S0960-9822(98)70299-4.
14. Li, L., Klim, J.R., Derda, R., Courtney, A.H., and Kiessling, L.L. (2011). Spatial control of cell fate using synthetic surfaces to potentiate TGF-β signaling. Proc. Natl. Acad. Sci. USA *108*, 11745–11750. https://doi.org/10.1073/pnas.1101454108.
15. Lin, L., Liu, L., Zhao, B., Xie, R., Lin, W., Li, H., Li, Y., Shi, M., Chen, Y.-G., Springer, T.A., and Chen, X. (2015). Carbon nanotube-assisted optical activation of TGF-β signalling by near-infrared light. Nat. Nanotechnol. *10*, 465–471. https://doi.org/10.1038/nnano.2015.28.
16. Singh, J., Chuaqui, C.E., Boriack-Sjodin, P.A., Lee, W.-C., Pontz, T., Corbley, M.J., Cheung, H.-K., Arduini, R.M., Mead, J.N., Newman, M.N., et al. (2003). Successful shape-Based virtual screening: the discovery of a potent inhibitor of the type I TGFβ receptor kinase (TβRI). Bioorg. Med. Chem. Lett. *13*, 4355–4359. https://doi.org/10.1016/j.bmcl.2003.09.028.
17. Kwiatkowski, W., Gray, P.C., and Choe, S. (2014). Engineering TGF-β superfamily ligands for clinical applications. Trends Pharmacol. Sci. *35*, 648–657. https://doi.org/10.1016/j.tips.2014.10.006.
18. Repina, N.A., Rosenbloom, A., Mukherjee, A., Schaffer, D.V., and Kane, R.S. (2017). At light speed: advances in optogenetic systems for regulating cell signaling and behavior. Annu. Rev. Chem. Biomol. Eng. *8*, 13–39. https://doi.org/10.1146/annurev-chembioeng-060816-101254.
19. Repina, N.A., McClave, T., Johnson, H.J., Bao, X., Kane, R.S., and Schaffer, D.V. (2020). Engineered illumination devices for optogenetic control of cellular signaling dynamics. Cell Rep. *31*, 107737. https://doi.org/10.1016/j.celrep.2020.107737.
20. Choi, I.Y., Lim, H., Huynh, A., Schofield, J., Cho, H.J., Lee, H., Andersen, P., Shin, J.H., Heo, W.D., Hyun, S.-H., et al. (2021). Novel culture system via wirelessly controllable optical stimulation of the FGF signaling pathway for human and pig pluripotency. Biomaterials *269*, 120222. https://doi.org/10.1016/j.biomaterials.2020.120222.
21. Humphreys, P.A., Woods, S., Smith, C.A., Bates, N., Cain, S.A., Lucas, R., and Kimber, S.J. (2020). Optogenetic control of the BMP signaling pathway. ACS Synth. Biol. *9*, 3067–3078. https://doi.org/10.1021/acssynbio.0c00315.
22. Repina, N.A., Bao, X., Zimmermann, J.A., Joy, D.A., Kane, R.S., and Schaffer, D.V. (2019). Optogenetic control of Wnt signaling for modeling early embryogenic patterning with human pluripotent stem cells. Bioengineering. https://doi.org/10.1101/665695.
23. Harradine, K.A., and Akhurst, R.J. (2006). Mutations of TGFß signaling molecules in human disease. Ann. Med. *38*, 403–414. https://doi.org/10.1080/07853890600919911.
24. Li, Y., Lee, M., Kim, N., Wu, G., Deng, D., Kim, J.M., Liu, X., Heo, W.D., and Zi, Z. (2018). Spatiotemporal control of TGF-β signaling with light. ACS Synth. Biol. *7*, 443–451. https://doi.org/10.1021/acssynbio.7b00225.
25. Dominici, M., Le Blanc, K., Mueller, I., Slaper-Cortenbach, I., Marini, F.C., Krause, D.S., Deans, R.J., Keating, A., Prockop, D.J., and Horwitz, E.M. (2006). Minimal criteria for defining multipotent mesenchymal stromal cells. The International Society for Cellular Therapy position statement. Cytotherapy *8*, 315–317. https://doi.org/10.1080/14653240600855905.

26. Benya, P.D., and Shaffer, J.D. (1982). Dedifferentiated chondrocytes reexpress the differentiated collagen phenotype when cultured in agarose gels. Cell *30*, 215–224. https://doi.org/10.1016/0092-8674(82)90027-7.

27. Xia, X., Zhang, Y., Zieth, C.R., and Zhang, S.-C. (2010). Transgenes delivered by lentiviral vector are suppressed in human embryonic stem cells in a promoter-dependent manner. Stem Cell. Dev. *16*, 167–176.

28. Jeon, E.S., Moon, H.J., Lee, M.J., Song, H.Y., Kim, Y.M., Bae, Y.C., Jung, J.S., and Kim, J.H. (2006). Sphingosylphosphorylcholine induces differentiation of human mesenchymal stem cells into smooth-muscle-like cells through a TGF-β-dependent mechanism. J. Cell Sci. *119*, 4994–5005. https://doi.org/10.1242/jcs.03281.

29. Bugaj, L.J., and Lim, W.A. (2019). High-throughput multicolor optogenetics in microwell plates. Nat. Protoc. *14*, 2205–2228. https://doi.org/10.1038/s41596-019-0178-y.

30. Liu, H., Zhang, C., Zhu, S., Lu, P., Zhu, T., Gong, X., Zhang, Z., Hu, J., Yin, Z., Heng, B.C., et al. (2015). Mohawk promotes the tenogenesis of mesenchymal stem cells through activation of the TGFβ signaling pathway. Stem Cell. *33*, 443–455. https://doi.org/10.1002/stem.1866.

31. Kuo, C.K., and Tuan, R.S. (2008). Mechanoactive tenogenic differentiation of human mesenchymal stem cells. Tissue Eng. *14*, 1615–1627. https://doi.org/10.1089/ten.tea.2006.0415.

32. Bakhshandeh, B., Soleimani, M., Paylakhi, S.H., and Ghaemi, N. (2012). A microRNA signature associated with chondrogenic lineage commitment. J. Genet. *91*, 171–182. https://doi.org/10.1007/s12041-012-0168-0.

33. Haseeb, A., Kc, R., Angelozzi, M., de Charleroy, C., Rux, D., Tower, R.J., Yao, L., Pellegrino da Silva, R., Pacifici, M., Qin, L., and Lefebvre, V. (2021). SOX9 keeps growth plates and articular cartilage healthy by inhibiting chondrocyte dedifferentiation/osteoblastic redifferentiation. Proc. Natl. Acad. Sci. USA *118*, e2019152118. https://doi.org/10.1073/pnas.2019152118.

34. Girardot, M., Bayet, E., Maurin, J., Fort, P., Roux, P., and Raynaud, P. (2018). SOX9 has distinct regulatory roles in alternative splicing and transcription. Nucleic Acids Res. *46*, 9106–9118. https://doi.org/10.1093/nar/gky553.

35. Clancy, B.M., Johnson, J.D., Lambert, A.-J., Rezvankhah, S., Wong, A., Resmini, C., Feldman, J.L., Leppanen, S., and Pittman, D.D. (2003). A gene expression profile for endochondral bone formation: oligonucleotide microarrays establish novel connections between known genes and BMP-2-induced bone formation in mouse quadriceps. Bone *33*, 46–63. https://doi.org/10.1016/S8756-3282(03)00116-9.

36. Bhumiratana, S., Eton, R.E., Oungoulian, S.R., Wan, L.Q., Ateshian, G.A., and Vunjak-Novakovic, G. (2014). Large, stratified, and mechanically functional human cartilage grown in vitro by mesenchymal condensation. Proc. Natl. Acad. Sci. USA *111*, 6940–6945. https://doi.org/10.1073/pnas.1324050111.

37. Bhumiratana, S., and Vunjak-Novakovic, G. (2015). Engineering physiologically stiff and stratified human cartilage by fusing condensed mesenchymal stem cells. Methods *84*, 109–114. https://doi.org/10.1016/j.ymeth.2015.03.016.

38. Lilledahl, M., Olderøy, M., Finnøy, A., Olstad, K., and Brinchman, J.E. (2015). Second harmonic generation imaging in tissue engineering and cartilage pathologies. In Multiphoton Microscopy in the Biomedical Sciences, *XV* (SPIE), pp. 145–150. https://doi.org/10.1117/12.2081583.

39. Bugaj, L.J., Sabnis, A.J., Mitchell, A., Garbarino, J.E., Toettcher, J.E., Bivona, T.G., and Lim, W.A. (2018). Cancer mutations and targeted drugs can disrupt dynamic signal encoding by the Ras-Erk pathway. Science *361*, eaao3048. https://doi.org/10.1126/science.aao3048.

40. Bugaj, L.J., Choksi, A.T., Mesuda, C.K., Kane, R.S., and Schaffer, D.V. (2013). Optogenetic protein clustering and signaling activation in mammalian cells. Nat. Methods *10*, 249–252. https://doi.org/10.1038/nmeth.2360.

41. Rosenbloom, A.B., Tarczyński, M., Lam, N., Kane, R.S., Bugaj, L.J., and Schaffer, D.V. (2020). β-Catenin signaling dynamics regulate cell fate in differentiating neural stem cells. Proc. Natl. Acad. Sci. USA *117*, 28828–28837. https://doi.org/10.1073/pnas.2008509117.

42. Hellwarth, P.B., Chang, Y., Das, A., Liang, P.-Y., Lian, X., Repina, N.A., and Bao, X. (2021). Optogenetic-mediated cardiovascular differentiation and patterning of human pluripotent stem cells. Adv. Genet. *2*, e202100011. https://doi.org/10.1002/ggn2.202100011.

43. Vila, O.F., Chavez, M., Ma, S.P., Yeager, K., Zholudeva, L.V., Colón-Mercado, J.M., Qu, Y., Nash, T.R., Lai, C., Feliciano, C.M., et al. (2021). Bioengineered optogenetic model of human neuromuscular junction. Biomaterials *276*, 121033. https://doi.org/10.1016/j.biomaterials.2021.121033.

44. Chua, C.J., Han, J.L., Li, W., Liu, W., and Entcheva, E. (2021). Integration of engineered "spark-cell" spheroids for optical pacing of cardiac tissue. Front. Bioeng. Biotechnol. *9*, 658594.

45. Rieger, M., Dellenbach, C., vom Berg, J., Beil-Wagner, J., Maguy, A., and Rohr, S. (2021). Enabling comprehensive optogenetic studies of mouse hearts by simultaneous opto-electrical panoramic mapping and stimulation. Nat. Commun. *12*, 5804. https://doi.org/10.1038/s41467-021-26039-8.

46. Wang, L., Cheng, Y., Wang, X., Rao, P., Li, H., Zheng, G., Li, Z., Jiang, C., Huang, C., Zhou, Q., et al. (2020). Near-infrared light driven tissue-penetrating cardiac optogenetics via upconversion nanoparticles in vivo. Biomed. Opt Express *11*, 1401–1416. https://doi.org/10.1364/BOE.381480.

47. Wu, X., Zhang, Y., Takle, K., Bilsel, O., Li, Z., Lee, H., Zhang, Z., Li, D., Fan, W., Duan, C., et al. (2016). Dye-sensitized core/active shell upconversion nanoparticles for optogenetics and bioimaging applications. ACS Nano *10*, 1060–1066. https://doi.org/10.1021/acsnano.5b06383.

48. Yadav, K., Chou, A.-C., Ulaganathan, R.K., Gao, H.-D., Lee, H.-M., Pan, C.-Y., and Chen, Y.-T. (2017). Targeted and efficient activation of channelrhodopsins expressed in living cells via specifically-bound upconversion nanoparticles. Nanoscale *9*, 9457–9466. https://doi.org/10.1039/C7NR03246C.

49. Yu, N., Huang, L., Zhou, Y., Xue, T., Chen, Z., and Han, G. (2019). Near-infrared-light activatable nanoparticles for deep-tissue-penetrating wireless optogenetics. Adv. Healthc. Mater. *8*, 1801132. https://doi.org/10.1002/adhm.201801132.

50. Hörner, M., Jerez-Longres, C., Hudek, A., Hook, S., Yousefi, O.S., Schamel, W.W.A., Hörner, C., Zurbriggen, M.D., Ye, H., Wagner, H.J., et al. Spatiotemporally confined red light-controlled gene delivery at single-cell resolution using adeno-associated viral vectors. Sci. Adv. 7, eabf0797. 10.1126/sciadv.abf0797.

51. Zhou, Y., Kong, D., Wang, X., Yu, G., Wu, X., Guan, N., Weber, W., and Ye, H. (2022). A small and highly sensitive red/far-red optogenetic switch for applications in mammals. Nat. Biotechnol. *40*, 262–272. https://doi.org/10.1038/s41587-021-01036-w.

52. Redchuk, T.A., Omelina, E.S., Chernov, K.G., and Verkhusha, V.V. (2017). Near-infrared optogenetic pair for protein regulation and spectral multiplexing. Nat. Chem. Biol. *13*, 633–639. https://doi.org/10.1038/nchembio.2343.

53. Redchuk, T.A., Kaberniuk, A.A., and Verkhusha, V.V. (2018). Near-infrared light–controlled systems for gene transcription regulation, protein targeting and spectral multiplexing. Nat. Protoc. *13*, 1121–1136. https://doi.org/10.1038/nprot.2018.022.

54. Redchuk, T.A., Karasev, M.M., Omelina, E.S., and Verkhusha, V.V. (2018). Near-infrared light-controlled gene expression and protein targeting in neurons and non-neuronal cells. Chembiochem *19*, 1334–1340. https://doi.org/10.1002/cbic.201700642.

55. Ashraf, J.V., and Al Haj Zen, A. (2021). Role of vascular smooth muscle cell phenotype switching in arteriogenesis. Int. J. Mol. Sci. *22*, 10585. https://doi.org/10.3390/ijms221910585.

56. Kelly-Goss, M.R., Sweat, R.S., Stapor, P.C., Peirce, S.M., and Murfee, W.L. (2014). Targeting pericytes for angiogenic therapies. Microcirculation *21*, 345–357. https://doi.org/10.1111/micc.12107.

57. Park, D., Spencer, J.A., Koh, B.I., Kobayashi, T., Fujisaki, J., Clemens, T.L., Lin, C.P., Kronenberg, H.M., and Scadden, D.T. (2012). Endogenous

bone marrow MSCs are dynamic, fate-restricted participants in bone maintenance and regeneration. Cell Stem Cell *10*, 259–272. https://doi.org/10.1016/j.stem.2012.02.003.

58. Bartold, M., Gronthos, S., Haynes, D., and Ivanovski, S. (2019). Mesenchymal stem cells and biologic factors leading to bone formation. J. Clin. Periodontol. *46*, 12–32. https://doi.org/10.1111/jcpe.13053.
59. Xu, M., Shaw, G., Murphy, M., and Barry, F. (2019). Induced pluripotent stem cell-derived mesenchymal stromal cells are functionally and genetically different from bone marrow-derived mesenchymal stromal cells. Stem Cell. *37*, 754–765. https://doi.org/10.1002/stem.2993.
60. Svoboda, D.S., Barrasa, M.I., Shu, J., Rietjens, R., Zhang, S., Mitalipova, M., Berube, P., Fu, D., Shultz, L.D., Bell, G.W., and Jaenisch, R. (2019). Human iPSC-derived microglia assume a primary microglia-like state after transplantation into the neonatal mouse brain. Proc. Natl. Acad. Sci. USA *116*, 25293–25303. https://doi.org/10.1073/pnas.1913541116.
61. Pavlovic, B.J., Blake, L.E., Roux, J., Chavarria, C., and Gilad, Y. (2018). A comparative assessment of human and chimpanzee iPSC-derived cardiomyocytes with primary heart tissues. Sci. Rep. *8*, 15312. https://doi.org/10.1038/s41598-018-33478-9.
62. Sahel, J.-A., Boulanger-Scemama, E., Pagot, C., Arleo, A., Galluppi, F., Martel, J.N., Esposti, S.D., Delaux, A., de Saint Aubert, J.-B., de Montleau, C., et al. (2021). Partial recovery of visual function in a blind patient after optogenetic therapy. Nat. Med. *27*, 1223–1229. https://doi.org/10.1038/s41591-021-01351-4.
63. Bansal, A., Shikha, S., and Zhang, Y. (2023). Towards translational optogenetics. Nat. Biomed. Eng. *7*, 349–369. https://doi.org/10.1038/s41551-021-00829-3.
64. Doehn, U., Hauge, C., Frank, S.R., Jensen, C.J., Duda, K., Nielsen, J.V., Cohen, M.S., Johansen, J.V., Winther, B.R., Lund, L.R., et al. (2009). RSK is a principal effector of the RAS-ERK pathway for eliciting a coordinate promotile/invasive gene program and phenotype in epithelial cells. Mol. Cell *35*, 511–522. https://doi.org/10.1016/j.molcel.2009.08.002.
65. Smeeton, J., Askary, A., and Crump, J.G. (2017). Building and maintaining joints by exquisite local control of cell fate. WIREs. Dev. Biol. *6*, e245. https://doi.org/10.1002/wdev.245.
66. Kathiriya, I.S., Rao, K.S., Iacono, G., Devine, W.P., Blair, A.P., Hota, S.K., Lai, M.H., Garay, B.I., Thomas, R., Gong, H.Z., et al. (2021). Modeling human TBX5 haploinsufficiency predicts regulatory networks for congenital heart disease. Dev. Cell *56*, 292–309.e9. https://doi.org/10.1016/j.devcel.2020.11.020.
67. Gerosa, L., Mazzoleni, S., Rusconi, F., Longaretti, A., Lewerissa, E., Pelucchi, S., Murru, L., Giannelli, S.G., Broccoli, V., Marcello, E., et al. (2022). The epilepsy-associated protein PCDH19 undergoes NMDA receptor-dependent proteolytic cleavage and regulates the expression of immediate-early genes. Cell Rep. *39*, 110857. https://doi.org/10.1016/j.celrep.2022.110857.
68. King, O., Cruz-Moreira, D., Sayed, A., Kermani, F., Kit-Anan, W., Sunyovszki, I., Wang, B.X., Downing, B., Fourre, J., Hachim, D., et al. (2022). Functional microvascularization of human myocardium in vitro. Cell Rep. Methods *2*, 100280. https://doi.org/10.1016/j.crmeth.2022.100280.
69. Thomas, O.S., Hörner, M., and Weber, W. (2020). A graphical user interface to design high-throughput optogenetic experiments with the optoPlate-96. Nat. Protoc. *15*, 2785–2787. https://doi.org/10.1038/s41596-020-0349-x.
70. Meier, F., Brunner, A.-D., Frank, M., Ha, A., Bludau, I., Voytik, E., Kaspar-Schoenefeld, S., Lubeck, M., Raether, O., Bache, N., et al. (2020). diaPASEF: parallel accumulation-serial fragmentation combined with data-independent acquisition. Nat. Methods *17*, 1229–1236. https://doi.org/10.1038/s41592-020-00998-0.
71. Kulak, N.A., Pichler, G., Paron, I., Nagaraj, N., and Mann, M. (2014). Minimal, encapsulated proteomic-sample processing applied to copy-number estimation in eukaryotic cells. Nat. Methods *11*, 319–324. https://doi.org/10.1038/nmeth.2834.
72. Adachi, J., Hashiguchi, K., Nagano, M., Sato, M., Sato, A., Fukamizu, K., Ishihama, Y., and Tomonaga, T. (2016). Improved proteome and phosphoproteome analysis on a cation exchanger by a combined acid and salt gradient. Anal. Chem. *88*, 7899–7903. https://doi.org/10.1021/acs.analchem.6b01232.
73. Bruderer, R., Bernhardt, O.M., Gandhi, T., Miladinović, S.M., Cheng, L.-Y., Messner, S., Ehrenberger, T., Zanotelli, V., Butscheid, Y., Escher, C., et al. (2015). Extending the limits of quantitative proteome profiling with data-independent acquisition and application to acetaminophen-treated three-dimensional liver microtissues. Mol. Cell. Proteomics *14*, 1400–1410. https://doi.org/10.1074/mcp.M114.044305.
74. Chen, D., Wu, J.Y., Kennedy, K.M., Yeager, K., Bernhard, J.C., Ng, J.J., Zimmerman, B.K., Robinson, S., Durney, K.M., Shaeffer, C., et al. (2020). Tissue engineered autologous cartilage-bone grafts for temporomandibular joint regeneration. Sci. Transl. Med. *12*, eabb6683. https://doi.org/10.1126/scitranslmed.abb6683.
75. Bhumiratana, S., Bernhard, J.C., Alfi, D.M., Yeager, K., Eton, R.E., Bova, J., Shah, F., Gimble, J.M., Lopez, M.J., Eisig, S.B., and Vunjak-Novakovic, G. (2016). Tissue-engineered autologous grafts for facial bone reconstruction. Sci. Transl. Med. *8*, 343ra83. https://doi.org/10.1126/scitranslmed.aad5904.
76. Grayson, W.L., Fröhlich, M., Yeager, K., Bhumiratana, S., Chan, M.E., Cannizzaro, C., Wan, L.Q., Liu, X.S., Guo, X.E., and Vunjak-Novakovic, G. (2010). Engineering anatomically shaped human bone grafts. Proc. Natl. Acad. Sci. USA *107*, 3299–3304. https://doi.org/10.1073/pnas.0905439106.

STAR★METHODS

KEY RESOURCES TABLE

REAGENT or RESOURCE	SOURCE	IDENTIFIER
Antibodies		
Anti-SOX2 antibody	Abcam	Cat# ab97959; RRID: AB_2341193
Anti-Oct4 antibody [EPR17929]	Abcam	Cat# ab181557; RRID: AB_2687916
Nanog (D73G4) XP Rabbit antibody	Cell signaling	Cat# 4903; RRID: AB_10559205
Goat Anti-Human Aggrecan Antigen Affinity-purified Polyclonal Antibody	R&D Systems	Cat# 967800
Goat Anti-Mouse FABP-4 Antigen Affinity-purified Polyclonal Antibody	R&D Systems	Cat# 967799
Alkaline Phosphatase antibody	Abcam	Cat# ab75699; RRID: AB_1309941
Cleaved Caspase-3 (Asp175) Antibody	Cell Signaling Technology	Cat# 9661; RRID: AB_2341188
Calponin 1 (D8L2T) XP® Rabbit mAb	Cell Signaling Technology	Cat# 17819; RRID: AB_2798789
Alpha-Smooth Muscle Actin Monoclonal Antibody (1A4)	ThermoFisher	Cat# 14-9760-82; RRID: AB_2572996
Rabbit Anti-SCXA, N Terminus Polyclonal Antibody, Unconjugated	Abcam	Cat# ab58655; RRID: AB_882467
COL1A1 (E3E1X) Mouse mAb	Cell Signaling Technology	Cat# 66948; RRID: AB_2920541
Anti-Clusterin antibody	Abcam	Cat# ab69644; RRID: AB_1267705
Anti-TGF beta Receptor I antibody	Abcam	Cat# ab235178; RRID: AB_2895230
Calponin 1 Antibody (CALP)	Santa Cruz Biotechnology	Cat# sc-58707; RRID: AB_781770
Bacterial and virus strains		
10-beta Competent E. coli (High Efficiency)	New England BioLabs	C3019H
Biological samples		
Bovine calf metacarpus bones	Lampire Biological Laboratories	N/A
Chemicals, peptides, and recombinant proteins		
Lenti-X Concentrator	Takara	Cat# 631232
Lenti-X Accelerator	Takara	Cat# 631257
Matrigel	Corning	Cat# 354234
EDTA	ThermoFisher	Cat# AM9261
Y-27632 dihydrochloride	Tocris	Cat# 1254
KaryoMAX Colcemid Solution	ThermoFisher	Cat# 15212012
Recombinant Human FGF-basic (154 a.a.)	Peprotech	Cat# 100-18B
TrypLE	ThermoFisher	Cat# 12605010
Halt Protease Inhibitor Cocktail	ThermoFisher	Cat# 78430
L-Ascorbic acid 2-phosphate sesquimagnesium salt hydrate	Sigma	Cat# A8960
Recombinant Human GDF-7	Peprotech	Cat# 120-37
Recombinant Human CTGF	Peprotech	Cat# 120-19
Human Transforming Growth Factor β3	Cell Signaling	Cat# 8425
Agarose, low gelling temperature	Sigma	Cat# A4018
ITS+ Premix Universal Culture Supplement	Corning	Cat# 354352
HEPES	Corning	Cat# 25060CI
Sodium Pyruvate	Corning	Cat# 25000CI
Dexamethasone	Sigma	Cat# D4902
L-Proline	Sigma	Cat# P5607
Fast SYBR Green Master Mix	ThermoFisher	Cat# 4385610
OSTEOSOFT	Sigma	Cat# 1.01728

(*Continued on next page*)

Continued

REAGENT or RESOURCE	SOURCE	IDENTIFIER
CitriSolv Hybrid Solvent and Clearing Agent	Fisher Scientific	Cat# 04-355-121
Hyaluronidase	Sigma	Cat# H6254
Hoechst 33342	Abcam	Cat# ab228551
Cytofix/Cytoperm	BD	Cat# 554722; RRID: AB_2869010
Deoxyribonuclease I	Sigma	Cat# D4263
Ribonuclease A	Sigma	Cat# R4875
Critical commercial assays		
E.Z.N.A. Endo-free Plasmid DNA Mini Kit I	Omega Bio-Tek	Cat# D6948-01
STEMdiff Mesenchymal Progenitor Kit	Stemcell Technologies	Cat# 05240
Human MSC Analysis Kit	BD	Cat# 562245
MSC Phenotyping Cocktail Kit, anti-human	Miltenyi	Cat# 130-095-198
Anti-Mouse Ig, κ/Negative Control Compensation Particles Set	BD	Cat# 552843
Human Mesenchymal Stem Cell Functional Identification Kit	R&D Systems	Cat# SC006
Pierce BCA Protein Assay Kit	ThermoFisher	Cat# 23225
RNeasy Micro Kit	Qiagen	Cat# 74004
High-Capacity cDNA Reverse Transcription Kit	ThermoFisher	Cat# 4368814
VECTASTAIN Elite ABC Universal PLUS Kit, Peroxidase (Horse Anti-Mouse/Rabbit IgG)	Vector Laboratories	Cat# PK-8200
CD90 MicroBeads, human	Miltenyi	Cat# 130-096-253
Deposited data		
Global quantitative proteomics raw datasets	This paper	ProteomeXchange: PXD040232
Experimental models: Cell lines		
HEK293T	ATCC	RRID: CVCL_0063
GM25256	Coriell	Cat# GM25256; RRID: CVCL_Y803
TGF-β Reporter HEK 293 Cells	InvivoGen	Cat# hkb-tgfb
Oligonucleotides		
GAPDH forward primer	Life Technologies	GCTCTCTGCTCCTCCTGTTC
GAPDH reverse primer	Life Technologies	ACCAAATCCGTTGACTCCGA
ASMA forward primer	Life Technologies	ACGTGGGTGACGAAGCACAG
ASMA reverse primer	Life Technologies	GGGCAACACGAAGCTCATTGTA
CNN1 forward primer	Life Technologies	GCTGTCAGCCGAGGTTAAGAA
CNN1 reverse primer	Life Technologies	TGAGGCCGTCCATGAAGTTG
SCX forward primer	Life Technologies	CAGCGGCACACGGCGAAC
SCX reverse primer	Life Technologies	CGTTGCCCAGGTGCGAGATG
COL1A1 forward primer	Life Technologies	TAAAGGGTCACCGTGGCT
COL1A1 reverse primer	Life Technologies	CGAACCACATTGGCATCA
Recombinant DNA		
pCMV-OptoTGFBRs	Addgene; gift from Dr. Won Do Heo	RRID: Addgene_118942
iRFP682-Smad2	Addgene; gift from Dr. Won Do Heo	RRID: Addgene_118943
pLV-EF1a-IRES-Neo	Addgene	RRID: Addgene_85139
Software and algorithms		
Benchling	https://benchling.com	RRID: SCR_013955
SnapGene	http://www.snapgene.com	RRID: SCR_015052

(*Continued on next page*)

Continued

REAGENT or RESOURCE	SOURCE	IDENTIFIER
FlowJo	https://www.flowjo.com/solutions/flowjo	RRID: SCR_008520
Spectronaut	https://biognosys.com/software/spectronaut/	N/A
NIS-Elements	https://www.nikoninstruments.com/Products/Software	RRID: SCR_014329
GraphPad	http://graphpad.com/	RRID: SCR_000306
Fiji	https://fiji.sc/	RRID: SCR_002285

RESOURCE AVAILABILITY

Lead contact

Further information and requests for resources and reagents should be directed to and will be fulfilled by the lead contact, Gordana Vunjak-Novakovic (gv2131@columbia.edu).

Materials availability

The lead contact may be contacted for material availability.

Data and code availability

- Proteomics data are deposited at ProteomeXchange: PXD040232 and are publicly available as of the date of publication. All other data used in this study are available from the lead contact upon request.
- This paper does not report original code.
- Any additional information required to reanalyze the data reported in this paper is available from the lead contact upon request.

EXPERIMENTAL MODEL AND SUBJECT DETAILS

Plasmid preparation

Retroviral plasmids containing tdTomato-tagged blue light-responsive TGF-β receptors (Addgene #118942) and iRFP682-tagged Smad2 (Addgene # 118943) were provided as a gift by Dr. Won Do Heo.[24] Transformed colonies of competent *E. coli* (C3019H; New England BioLabs) were selected, amplified, and purified (E.Z.N.A. Endo-Free Plasmid DNA Kit; Omega Bio-Tek). Omitting the retroviral backbone, lentiviral plasmids were designed using Benchling and SnapGene software and constructed using custom cloning service of Epoch Life Science. The sequences for the light-responsive TGF-β receptors and iRFP682-Smad2 were inserted separately into lentiviral backbones (pLV-EF1a-IRES-Neo; Addgene #85139). The lentiviral plasmids were similarly amplified and purified.

Lentiviral transduction and stable hiPSC line generation

Human embryonic kidney (HEK) 293T cells (ATCC) were cultured in high-glucose Dulbecco's modified Eagle's medium (hgDMEM; Gibco), 10% (v/v) Tet System Approved fetal bovine serum (FBS; Takara), 1 mM sodium pyruvate (Corning), and 1X GlutaMAX (Gibco) with media changes twice per week until reaching approximately 70% confluency. All human cells were maintained in a 37°C and 5% CO_2 incubator. Packaged lentiviral vector plasmid DNA (Lenti-X Packaging Single Shots; Takara) was added to the culture per manufacturer's protocol and virus supernatant was harvested after 48 and 72 h. Stocks were pooled, filtered to remove cellular debris (0.45 μm pore size PVDF membrane vacuum filter; Millipore Sigma) and concentrated (Lenti-X Concentrator; Takara).

hiPSCs (GM25256; Coriell) were cultured on plates coated with Matrigel (Corning) diluted 1:175 in Roswell Park Memorial Institute (RPMI) 1640 Medium (Gibco), for 30 min at 37°C. hiPSCs were maintained in mTeSR Plus (STEMCELL Technologies) with media changes every other day. Upon reaching approximately 70% confluency, hiPSCs were dissociated using 500 μM ethylenediaminetetraacetic acid (EDTA; Thermo Fisher) and passaged in the presence of 5 mM ROCK inhibitor (Y-27632 2HCl; Tocris Bioscience).

Fresh viral titers were used to transduce hiPSC cultures (Lenti-X Accelerator; Takara) 1 day after passaging, then ROCK inhibitor was removed. Expression of vector plasmid DNA in target cells was verified by fluorescent microscopy (Olympus IX81) after 3 days. Colonies expressing tdTomato were manually picked, dissociated, resuspended in fluorescence-activated cell sorting (FACS) buffer comprised of phosphate-buffered saline (PBS; Corning) with 2% (v/v) FBS and 1 mM EDTA, and filtered through a 70 μm cell strainer. After single-cell sorting (BD FACSAria), cells were clonally expanded (CloneR; STEMCELL Technologies) to establish stable optogenetic hiPSC lines. For G-banded karyotyping, hiPSCs were treated with KaryoMAX colcemid solution (Gibco) for 2 h before dissociation and single cell resuspension in mTeSR Plus.

METHOD DETAILS

hiPSC to MSC differentiation

hiPSCs were differentiated into MSCs following manufacturer's protocol in the STEMdiff Mesenchymal Progenitor Kit (STEMCELL Technologies). Briefly, hiPSCs were passaged under standard conditions 2 days prior to starting a 4-day induction into early mesodermal progenitors. To derive mesenchymal progenitors, cells were then switched to the supplied MesenCult medium and passaged without using animal components to reach an approximately 70% confluency each time.

After the 21-day differentiation period, hiPSC-derived MSCs (hiMSCs) were cultured in MSC medium comprised of hgDMEM, 10% (v/v) fetal bovine serum (Corning), 1% (v/v) penicillin/streptomycin (P/S; Gibco), and 0.1 ng/mL fibroblast growth factor (Peprotech) with media changes twice per week on uncoated tissue culture plastic. hiMSCs were dissociated using TrypLE (Gibco) and cryopreserved with NutriFreez D10 (Biological Industries).

Flow cytometry for MSC cell surface markers

To analyze MSC cell surface markers by flow cytometry, hiMSCs were dissociated and resuspended at 5×10^6 cells/mL in FACS buffer, and filtered through a 70 μm cell strainer. Using a human MSC analysis kit (BD Biosciences), cells were labeled with an antibody cocktail for positive markers containing APC anti-CD73, FITC anti-CD90, and PerCP-Cy5.5 anti-CD105 for 30 min, then washed and resuspended in buffer. Due to interference between the fluorescent tdTomato tag on optogenetic cells and the PE conjugated antibody cocktail for negative markers, another human MSC phenotyping kit (Miltenyi Biotec) was used to analyze lineage markers with PerCP anti-CD34, CD45, CD14, CD19, and HLA-DR. Unstained cells, single-color stained compensation beads (CompBead Plus Anti-Mouse Ig, κ; BD Biosciences), and isotype antibody cocktails controls were also included. Live cells were immediately run on the flow cytometer (Bio-Rad ZE5) using 5×10^5 cells per sample. Subsequent analyses were carried out using the FlowJo software. Samples were gated for tdTomato-positive single cells against the corresponding isotype control, such that <5% isotype was positive.

Tri-differentiation of MSCs

Optogenetic and non-optogenetic hiMSCs were compared for their tri-differentiation potential into adipogenic, osteogenic, and chondrogenic lineages using an hMSC functional identification kit per manufacturer's protocol (R&D Systems).

For adipogenic differentiation, cells were dissociated and replated at 2.1×10^4 cells/cm^2 in the supplied adipogenic basal medium on cover glass bottom 24-well cell imaging plates (Eppendorf), cultured to 100% confluency, then switched to the supplied adipogenic differentiation medium. After 21 days of culture with medium changes every 3–4 days, adipocytes were fixed for immunostaining.

For osteogenic differentiation, cells were dissociated and replated at 4.2×10^3 cells/cm^2 in the supplied osteogenic basal medium on cover glass bottom 24-well cell imaging plates (Eppendorf) which had been coated with 1 μg/mL fibronectin (R&D Systems) for 3 h at 37°C. Cells were cultured to 50% confluency, then switched to the supplied osteogenic differentiation medium. After 21 days of culture with medium changes every 3–4 days, cells were fixed for immunostaining.

For chondrogenic differentiation, cells were dissociated and resuspended at 2.5×10^5 cells/mL in the supplied chondrogenic differentiation medium. Cell suspension was aliquoted at 1 mL per well into a deep-well U-bottom 96-well plate (Thermo Fisher), centrifuged at 200g for 5 min, and placed directly into the incubator to allow for self-assembly into condensed mesenchymal bodies over 2 days. After 21 days of culture with medium changes every 2–3 days, chondrogenic pellets were fixed for immunostaining.

Western Blot for TGFBR

Cell lysates were prepared in Pierce RIPA Lysis and Extraction Buffer with Halt Protease Inhibitor Cocktail, and protein concentrations were quantified using the Pierce BCA Protein Assay Kit (Thermo Fisher). 25 μg of protein in Laemmli Buffer was loaded in each lane of a 4–20% precast polyacrylamide gel, along with a Precision Plus Protein Dual Color ladder (Bio-Rad). The gel was transferred to a 0.45 μM polyvinylidene difluoride membrane, then the membrane was stained using Revert 700 (LI-COR) total protein stain, blocked in 5% bovine serum albumin (BSA) in Tris-Buffered Saline, 0.1% Tween 20 Detergent (TBST; Sigma), and incubated with an anti-TGFBR1 antibody (abcam ab235178, 1:1000) recognizing the extracellular region of TGFBR1.

Blue light optogenetic stimulation

Confocal laser stimulation and imaging were carried out on a multiphoton confocal microscope (Nikon A1RMP) with a live cell chamber, where cells were imaged first at baseline for 3 min without stimulation, then exposed to a 1–15 s pulses of 488 nm laser with 30 s imaging cycles, for up to 40 min total.

Longer-term light stimulation was carried out on an optogenetic stimulation device designed by following the reported system[29] and manufactured by PCB Unlimited. The device is compatible with incubator culture, readily adaptable for any well plate format, consisting of 192 individually programmable blue LEDs (OSRAM LB T64G-V1CA-59-Z), diffusers to distribute light evenly across the well (Grafix K07MM1824-10, 40W CO_2 laser cutter), a black plate adapter (McMaster-Carr 8545K1, CNC machined) and black lid to limit spillover between wells. The 96-well plate format was constructed and used for hydrogel experiments (chondrogenic

differentiations) to reduce cell requirements. In addition, the corresponding adapter for a 24-well plate format was designed and used for monolayer experiments (smooth muscle and tenogenic differentiations) to allow for sufficient RNA quantity for qRT-PCR.

The 488 nm light output at each position of the optogenetic stimulation device was measured with a handheld optical power and energy meter (THORLABS PM100D) with a photodiode power sensor (THORLABS S130VC) at the 0.5 mW setting. The photometer was fit with adapters for the well-plate format to measure actual light intensity per well. Parameters for each position of the light stimulation device (illumination time, light intensity) were programmed in Arduino with the optoConfig graphical user interface.[69]

Smooth muscle and tenogenic differentiations

optohiMSCs were dissociated and replated in MSC medium on cover glass bottom 24-well cell imaging plates (Eppendorf) to reach approximately 70% confluency after 2 days, then switched to induction medium for smooth muscle or tenogenic differentiation. Basal smooth muscle medium consisted of hgDMEM with 5% (v/v) FBS and 1% (v/v) P/S.[8] Basal tenogenic medium was supplemented with additional factors: 50 μg/mL ascorbic acid 2-phosphate (Sigma), 100 ng/mL human recombinant growth/differentiation factor-7 (GDF-7; Peprotech), and after 3 days, 100 ng/mL human recombinant connective tissue growth factor (CTGF; Peprotech).[9] A HEK293 secreted embryonic alkaline phosphatase (SEAP)-based reporter assay (Invivogen) was used to verify that the FBS used did not contain detectable levels of TGF-β (Figure S5). Individual wells were subjected to one of the following conditions.

(1) no soluble TGF-β or optogenetic stimulation,
(2) soluble human recombinant TGF-β3 (Cell Signaling) alone at 10 ng/mL,
(3) optogenetic stimulation alone with 5-min pulses every 2 h at 3 μW/1.9 cm^2
(4) optogenetic stimulation alone with 5-min pulses every 2 h at 6 μW/1.9 cm^2.

The respective basal smooth muscle or tenogenic medium was changed every 3 days over 14 days total. Samples were freshly isolated for RNA or fixed for immunostaining.

Chondrogenic differentiation

Sterile 4% (w/v) agarose solution was prepared by dissolving low gelling temperature agarose (Sigma) in PBS and autoclaving. The agarose solution was maintained at 41°C in a water bath. hiMSCs were passaged, counted, and resuspended in MSC medium at a concentration of 40 × 10^6 cells/mL. Agarose solution and cell suspension were mixed at a 1:1 ratio and pipetted into an autoclave-sterilized casting mold comprised of a 1.5 mm-thick U-shaped rubber gasket clamped between two plain glass microscope slides. The 2% (w/v) agarose solution containing 20 × 10^6 cells/mL was allowed to gel for 10 min at room temperature before being removed from the casting mold. Individual 6 mm-diameter × 1.5 mm thick gel discs were biopsy punched, deposited into separate wells of an ultra-low attachment plate, and maintained in MSC medium for at least 2 days.

Hydrogels were then transferred to individual wells of a cover glass bottom 96-well cell imaging plates (Cellvis) and switched to basal chondrogenic medium consisting of hgDMEM, 1% (v/v) P/S, 1% (v/v) insulin-transferrin-selenium mix (Corning), 10 mM 4-(2-hydroxyethyl)-1-piperazineethanesulfonic acid (HEPES; Corning), 0.9 mM sodium pyruvate (Gibco), 100 nM dexamethasone (Sigma), 50 μg/mL L-proline (Sigma), and 50 μg/mL ascorbic acid 2-phosphate (Sigma). Hydrogels were then subjected to one of the following conditions.

(1) no soluble TGF-β or optogenetic stimulation,
(2) soluble human recombinant TGF-β3 (Cell Signaling) alone at 10 ng/mL,
(3) optogenetic stimulation alone with 5-min pulses every 2 h at 3 μW/0.32 cm^2, or
(4) optogenetic stimulation alone with 5-min pulses every 2 h at 6 μW/0.32 cm^2.

For all groups, chondrogenic medium was changed every 3 days over 21 days of culture. Samples were snap frozen in liquid nitrogen for proteomics.

RNA isolation and qPCR analysis

RNA from cell monolayers was isolated using the RNeasy Micro Kit (QIAGEN) following manufacturer's protocol with on-column DNase treatment. RNA was quantified on a spectrophotometer (NanoDrop 1000; Thermo Fisher). cDNA was synthesized using the High-Capacity cDNA Reverse Transcription Kit (Applied Biosystems). Quantitative RT-PCR analysis was performed using 10 ng cDNA per reaction, Fast SYBR Green PCR Master Mix (Applied Biosystems), and primers synthesized by Life Technologies (Table S1). ΔCt was taken between the gene of interest and housekeeping gene *GAPDH*. ΔΔCt was calculated between the mean Ct values of technical replicates for each sample, and the average ΔCt for the control group. Fold change data were reported as $2^{-\Delta\Delta Ct}$.

Immunostaining

Monolayer samples were fixed for 15 min at room temperature and tissue samples were fixed overnight at 4°C in 4% (v/v) paraformaldehyde. Bone-containing samples were decalcified in OSTEOSOFT (Millipore Sigma) for 48 h at room temperature on an orbital shaker. Tissue samples were embedded in paraffin, and sectioned at 8 μm-thick. Monolayers were permeabilized in 0.25% (v/v)

Triton X-(Sigma) and 5% (v/v) FBS for 20 min at room temperature. Paraffin-embedded sections were baked for 30 min at 60°C, then deparaffinized and rehydrated in Citrisolv (Fisher Scientific) followed by a graded ethanol series. Antigen retrieval was performed in citrate buffer (10 mM sodium citrate, pH 6.0) heated to boiling for 20 min and cooled for another 20 min, followed by incubation in ~700 U/mL hyaluronidase in PBS (Sigma) for 15 min at 37°C. Sections were permeabilized for 20 min at room temperature in 0.25% (v/v) Triton and 5% (v/v) serum. For all samples, blocking was done using 10% (v/v) secondary antibody-matched serum for 2 h at room temperature. Primary antibodies in blocking solution were incubated on samples overnight at 4°C (please see Table S2 for antibodies and their dilutions). To show the specificity of the antibody binding, negative controls were stained without primary antibodies. For immunofluorescent staining, secondary antibodies were all prepared at 1:1000 dilution in 5% (v/v) serum and incubated for 2 h at room temperature, then nuclear staining was performed with Hoechst 33342 (Abcam). For immunohistological staining, subsequent steps with BLOXALL endogenous peroxidase quenching solution, biotinylated secondary antibody, ABC Reagent, and DAB Reagent were carried out per manufacturer's protocol (VECTASTAIN PK-8200; Vector Laboratories). Monolayer wells were maintained in PBS, while paraffin sections were dehydrated and cleared in a graded ethanol series followed by Citrisolv (Fisher Scientific) and mounted under cover glass with Permount (Fisher Scientific). Fluorescent images were acquired on a multiphoton confocal microscope (Nikon A1RMP). Color images at high magnification (20x) were taken of entire slides using an Olympus BX61VS.

Global quantitative proteomic analysis

For global quantitative proteomics, diaPASEF (data independent acquisition based proteomics) was used.[70] In brief, hydrogel encapsulated cells were lysed in buffer (1% SDC, 100 mM TrisHCl pH 8.5, and protease inhibitors) and boiled for 10 min at 95°C, 1500 rpm.[71] Protein reduction and alkylation of cysteines was performed with 10 mM TCEP and 40 mM CAA at 45°C for 10 min followed by sonication in a water bath, cooled down to room temperature. Protein digestion was processed overnight by adding LysC and trypsin in a 1:50 ratio (μg of enzyme to μg of protein) at 37°C and 1400 rpm. Peptides were acidified by adding 1% TFA, vortexed, and subjected to StageTip clean-up via SDB-RPS.[72] Peptides were loaded on 14-gauge StageTip plugs. Peptides were washed two times with 200 μL 1% TFA 99% ethyl acetate followed 200 μL 0.2% TFA/5% ACN in centrifuge at 3000 rpm, followed by elution with 60 μL of 1% Ammonia, 50% ACN into Eppendorf tubes and dried at 45°C in a SpeedVac centrifuge. Samples were resuspended in 10 μL of LC buffer (3% ACN/0.1% FA). Peptide concentrations were determined using NanoDrop and 200 ng of each sample was used for diaPASEF analysis on timsTOFPro.

Peptides were separated within 120 min at a flow rate of 400 nL/min on a reversed-phase C18 column with an integrated CaptiveSpray Emitter (25 cm × 75μm, 1.6 μm, IonOpticks). Mobile phases A and B were with 0.1% formic acid in water and 0.1% formic acid in ACN. The fraction of B was linearly increased from 2 to 23% within 90 min, followed by an increase to 35% within 10 min and a further increase to 80% before re-equilibration. The timsTOF Pro was operated in diaPASEF mode[70] and data was acquired at defined 32 × 25 Th isolation windows from m/z 400 to 1,200. To adapt the MS1 cycle time in diaPASEF, the repetitions were set to 2 in the 16-scan diaPASEF scheme. The collision energy was ramped linearly as a function of the mobility from 59 eV at 1/K0 = 1.6 Vs. cm-2 to 20 eV at 1/K0 = 0.6 Vs. cm^{-2}.

The acquired diaPASEF raw files were searched at default settings for targeted analysis of DIA data against the human UniProt fasta database in Spectronaut.[73] The false discovery rate (FDR) was estimated using the mProphet approach and set to 1% at peptide precursor level and at 1% at protein level. Results obtained from Spectronaut were further analyzed using the Spectronaut statistical package. Significantly changed protein abundance was determined by un-paired t test with a threshold for significance of $p < 0.05$ (permutation-based FDR correction) and 0.58 log_2FC.

Cartilage-bone tissue formation

Bovine calf metacarpus bones were purchased from Lampire Biological Laboratories (19D24003) and stored at −40°C. Using a vertical band saw, bone pieces were cut into smaller slices approximately 1 cm thick from the distal end of the metatarsal, as this region contains an enriched concentration of trabecular bone. From the 1 cm thick slices of bone, a drill press with a core drill bit was used to isolate cylindrical bone cores 3.5 mm in diameter (Figure S7A). The cores were then fed into an IsoMet low speed precision saw to trim each individual piece into 5.5 mm tall bone scaffolds with flat ends. The scaffolds were stripped of all cellular material to leave behind the extracellular matrix with largely preserved composition, architecture, and mechanical properties using previously described methodology.[74–76] Bones were washed with high-velocity streams of water to remove the marrow from the pore spaces, and treated on an orbital shaker in four steps to remove any remaining cellular material: (i) phosphate-buffered saline (PBS; Corning) with 0.1% EDTA (w/v) for 1 h at room temperature; (ii) hypotonic buffer of 10 mM Tris (Sigma), 0.1% EDTA (w/v) in DI water) overnight at 4°C; (iii) detergent (10 mM Tris, 0.5% SDS (w/v; Sigma) in DI water) for 24 h at room temperature; (iv) enzymatic solution (100 U/mL DNase, 1 U/mL RNase, 10 mM Tris in DI water; Sigma) for 6 h at 37°C. Sonication was used to remove any remaining debris from the scaffolds. After freeze-drying, decellularized bone scaffolds were weighed. Scaffolds of similar density were chosen for cell seeding (30–35 mg) and stored in 70% ethanol (v/v) for sterilization. Prior to cell seeding, ethanol was aspirated from the scaffolds and replaced with high-glucose Dulbecco's modified Eagle's medium (DMEM; Gibco) for at least 2 h.

The cartilaginous layer was generated from condensed mesenchymal bodies (CMBs) using our previously established protocol.[74] Briefly, hiMSCs were suspended at 2.5 × 10^5 cells/mL in chondrogenic medium containing 10 ng/mL TGF-β3 (Cell Signaling). Cell

suspension was aliquoted at 1 mL per well into a deep-well U-bottom 96-well plate (Thermo Fisher), centrifuged at 200g for 5 min, and placed directly into the incubator to allow for self-assembly into CMBs over 3 days with daily media changes (Figure S7A).

To form the tissues, the bone component of the setup consisted of a decellularized bone scaffold compressively secured about its cylindrical surface within a custom designed CNC machined polyetherimide (McMaster-Carr 7612K51) support structure. Selective compressive fixturing was enabled by installation of an O-ring. The cartilage region was sized to 2 mm thick (1 mm external to the scaffold with 1 mm penetrance into the bone) forming a flat, circular surface 3.5 mm in diameter. For each scaffold, this corresponded to approximately 37 spherical CMBs 1 mm in diameter or 21 spherical CMBs 1.2 mm in diameter. The specific CMB diameter was measured prior to tissue seeding to account for some variability between batches.

The cartilage component of the tissue forming setup consisted of a CNC machined white polytetrafluoroethylene (PTFE) (McMaster-Carr 8545K1) chamber to hold CMBs, a CNC machined polyetherimide (McMaster-Carr 7612K51) support piece at the base of the chamber with a set of six 1 mm-diameter channels to allow nutrient exchange, and a porous hydrophobic polycarbonate track-etched membrane filter (1 μm pore size, Sterlitech) clamped between the body of the chamber and the supporting base (Figure S7B). Once the appropriate number of CMBs were deposited into the chamber, the decellularized bone scaffold with predetermined height setting was pressed onto the cartilage layer.

The footprint of the cartilage-bone reactor was matched to a 24-well plate, with leftover working volume allowing the addition of sufficient media volume. From preliminary studies, it was determined that the CMBs needed 3 weeks in the confined culture setup to fuse and establish sufficient mechanical stability. During this time, complete chondrogenic medium containing TGF-β3 was changed twice weekly.

Subsequently, tissues were removed from confined culture within the cartilage chamber of the tissue forming setup (Figure S7C). Within their bone holders, tissues were placed on top of CNC machined polyetherimide (McMaster-Carr 7612K51) suspension platforms which allowed for free-swelling and light-accessible culture in black cover glass bottom 24-well cell imaging plates (Eppendorf). The superficial surface of the cartilage was oriented facing the bottom of the well such that it would receive the greatest light intensity when the well-plate was placed on top of the optogenetic stimulation device. Chondrogenic medium containing TGF-β3 was changed twice weekly.

Second harmonic generation imaging

Unstained 8 μm-thick histological sections were deparaffinized and mounted under cover glass with Permount (Fisher Scientific). Second harmonic generation imaging was carried out on a multiphoton confocal microscope (Nikon A1RMP) with a fundamental laser excitation wavelength of 820 nm at laser power of 2978 mW. Acquired XY frames with 15% overlap were stitched together using the Nikon NIS-Elements ND Processing Stitch Multipoint to Large Image function.

Non-optogenetic and optogenetic hiMSC Co-Culture

Starting from magnetically sorted CD90+ populations (Miltenyi Biotec) non-optogenetic and optogenetic populations of hiMSCs were dissociated and replated at a 2:1 ratio in MSC medium on cover glass bottom 24-well cell imaging plates (Eppendorf) to reach approximately 70% confluency after 2 days. The hiMSC co-cultures were then switched to induction medium for smooth muscle differentiation, with either.

(1) soluble human recombinant TGF-β3 (Cell Signaling) alone at 10 ng/mL, or
(2) optogenetic stimulation alone with 5-min pulses every 2 h at 3 μW/1.9 cm^2.

The smooth muscle medium was changed every 3 days. Non-optogenetic and optogenetic populations of hiMSCs which were maintained in co-culture in MSC medium for only 2 days were used as controls. After 2 weeks, co-cultures (n = 3) were analyzed by flow cytometry as before, with samples being fixed and permeabilized (Cytofix/Cytoperm; BD Biosciences) prior to staining for intracellular marker calponin-1 with Alexa Fluor 488 anti-calponin-1 (Santa Cruz Biotechnologies sc-58707, 1:100).

QUANTIFICATION AND STATISTICAL ANALYSIS

Statistical analysis for qPCR and flow cytometry data was conducted using GraphPad Prism software. Data were checked for whether they fit Gaussian distributions using the Shapiro-Wilk normality test. When normality was confirmed, statistical analysis was carried out by one-way analysis of variance (ANOVA) test and post hoc Tukey-Kramer's multiple comparisons test to compare groups (qPCR: *CNN1, COL1A1, SCX*; flow cytometry: calponin). When normality was not confirmed, statistical analysis was carried out by nonparametric Kruskal-Wallis test and post hoc Dunn's multiple comparisons test to compare groups (qPCR: *ASMA*). Data were expressed as the mean ± SD using data from $n \geq 6$ qPCR replicates and $n \geq 3$ flow cytometry replicates (as indicated in the figure legends). $p < 0.05$ was considered statistically significant.